

## Homochiral Columns Constructed by Chiral Self-Sorting During Supramolecular Helical Organization of Hat-Shaped Molecules

Cécile Roche,<sup>†</sup> Hao-Jan Sun,<sup>†,‡</sup> Margaret E. Prendergast,<sup>†</sup> Pawaret Leowanawat,<sup>†</sup> Benjamin E. Partridge,<sup>†</sup> Paul A. Heiney,<sup>‡</sup> Fumito Araoka,<sup>§</sup> Robert Graf,<sup>||</sup> Hans W. Spiess,<sup>||</sup> Xianbingong Zeng,<sup>⊥</sup> Goran Ungar,<sup>⊥,#</sup> and Virgil Percec<sup>\*,†</sup>

<sup>†</sup>Roy & Diana Vagelos Laboratories, Department of Chemistry, University of Pennsylvania, Philadelphia, Pennsylvania 19104-6323, United States

<sup>‡</sup>Department of Physics and Astronomy, University of Pennsylvania, Philadelphia, Pennsylvania 19104-6396, United States

<sup>§</sup>RIKEN Center for Emergent Matter Science, 2-1 Hirosawa, Wako, Saitama 351-0198, Japan

<sup>||</sup>Max-Planck Institute for Polymer Research, Mainz 55128, Germany

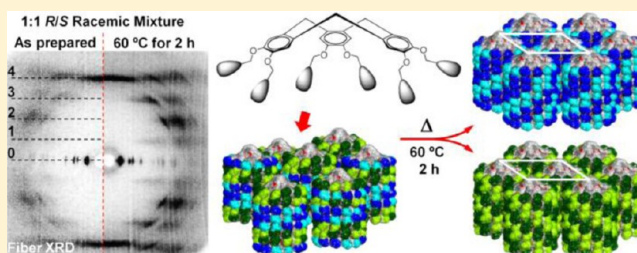
<sup>⊥</sup>Department of Materials Science and Engineering, University of Sheffield, Sheffield S1 3JD, United Kingdom

<sup>#</sup>Department of Physics, Zhejiang Sci-Tech University, Hangzhou 310018, China

### **S** Supporting Information

**ABSTRACT:** A library of dendronized cyclotrimeratrylene (CTV) crowns substituted with chiral, racemic, or achiral peripheral alkyl chains, including enantiopure *R* and *S* branched alkyls, “racemic by mixture”, “racemic by synthesis”, *n*-octyl, and *n*-dodecyl groups was synthesized. In solvophobic solvents and in bulk they self-assemble in helical columns. Their solution and bulk shape-persistent supramolecular structures were determined by a complementary combination of circular dichroism (CD) and UV in solution and thin film, microspot CD in thin film, differential scanning calorimetry

combined with fiber X-ray diffraction, computer simulation, and molecular models. In solution, self-assembly via a cooperative mechanism generates single-handed columns from enantiopure CTVs and mixtures of right- and left-handed columns from racemic by mixture, racemic by synthesis, other combinations of *R* and *S*, and even from achiral compounds. In bulk state all supramolecular columns form a 3D hexagonal crystalline phase,  $\Phi_h^k$  ( $P6_3$  symmetry), that can be obtained only from single-handed columns and a columnar hexagonal 2D liquid crystal,  $\Phi_h$ . The highest order  $\Phi_h^k$  consists of enantiopure single-handed columns that are slightly distorted 12-fold triple helices. The “hat-shaped” dendronized CTV assembles in bent-branch pine-tree columns that allow interdigitation of alkyl groups in adjacent columns regardless of their direction. Enantiomerically rich, racemic, and achiral compositions undergo deracemization in the crystal state by transfer of the transient disc-like conformer of dendronized CTV from column to column during crown inversion. Solid state NMR experiments identified motional processes that allow such transfer. This unprecedented supramolecular chiral self-sorting will impact the creation of functions in complex systems.



## ■ INTRODUCTION

Most natural compounds and biomacromolecules are homochiral. The origin of biological homochirality has fascinated the scientific community for centuries,<sup>1</sup> and the significance of homochirality is accepted in biology,<sup>1</sup> complex natural products,<sup>2a–c</sup> and pharmaceuticals.<sup>2d</sup> Since the pioneering experiment of Pasteur,<sup>3a</sup> the mechanisms of crystallization of low molar mass racemic organic compounds,<sup>3b</sup> their deracemization,<sup>3,4</sup> how to accomplish it,<sup>5</sup> and more recently the enantioselective synthesis<sup>6</sup> have become established fields. However, the generation and mechanisms of action of molecular and supramolecular chirality in the creation of supramolecular chiral assemblies are more recent and complex topics of research.<sup>7–9</sup> Creation of supramolecular chirality

involves mechanisms of transfer and amplification of structural information mediated by a helical arrangement of building blocks. The complexity of these mechanisms has only begun to be elucidated.<sup>8</sup> Crystallization of supramolecular homochiral and racemic systems as well as their deracemization entails the development of methodologies that are available for molecular but not supramolecular systems.<sup>6</sup> Knowledge from these developments will impact many areas of supramolecular chemistry and materials including organic electronics,<sup>10</sup> biological mimics, and many others. Therefore, the models required to study various classes of self-assembling building

Received: April 8, 2014

Published: April 23, 2014

blocks, their supramolecular structures, and their role in the understanding of fundamental concepts that mediate functions in complex systems are in demand.<sup>10</sup>

Our laboratory developed a class of dendritic dipeptides that self-assemble into porous helical transmembrane protein mimics that are persistent both in solution and in the solid state.<sup>11</sup> Therefore, their self-assembly could be investigated by a combination of complementary solution and solid state techniques.<sup>1c,12</sup> The role of all stereochemical permutations of a dendritic dipeptide, including homochiral, heterochiral, and differentially racemized variants, on the mechanism and thermodynamics of self-assembly was reported.<sup>1c,12</sup> This study demonstrated that the highest degree of stereochemical purity, enantiopure homochiral dendritic dipeptides, provides the most thermodynamically favorable self-assembly process in solution, corresponding to the greatest degree of order and crystallization in the solid state.<sup>12a</sup> Due to the high enthalpy of supramolecular helical polymerization mediated by a network of H-bonding and other interactions, these structures, including those generated with the lowest stereochemical purity, are more closely related to covalent rather than supramolecular polymers and subsequently do not undergo deracemization in the solid state. Therefore, while these experiments demonstrated the need of biological homochirality<sup>1c,12</sup> by showing that heterochiral and racemic systems provide less perfect assemblies that would not resemble the homochiral world in which we inhabit, they did not generate models to investigate the mechanism of racemization and deracemization. Deracemization experiments, also known as spontaneous optical resolution or chiral self-sorting, would require a more dynamic and weakly interacting model that also creates supramolecular assemblies persistent in solution and in the solid state.

Dendronized cyclotrimeratrylenes (CTV) provide weakly interacting and dynamic dendritic crowns that self-assemble into helical columns and spheres<sup>13</sup> resembling the structure of the cross-section of the helical columns assembled from dendritic dipeptides.<sup>11,12</sup> The flexible dendronized CTV undergoes crown inversion both in solution and in the bulk state.<sup>13b</sup> Therefore, the pine-tree helical columns assembled from CTV derivatives are expected to provide access to the mechanisms of formation of chiral supramolecular columns and their racemization and deracemization. This publication reports the first study of the mechanism and thermodynamics of self-assembly in solution and self-organization in the solid state of enantiomerically pure homochiral, several different mixtures of homochiral, two different chiral racemic, and achiral CTV derivatives dendronized with the smallest possible amphiphilic "minidendron"<sup>7m,9b</sup> to accomplish fast dynamics. Together with the first demonstration of deracemization or spontaneous optical resolution of supramolecular assemblies in the crystal state this study will demonstrate that dendronized CTV provides an excellent model for investigation of racemization and deracemization during supramolecular helical polymerization into complex columnar systems.

## RESULTS AND DISCUSSION

**Synthesis of Chiral and Achiral Dendronized Cyclotrimeratrylenes.** The structures of the dendronized CTV derivatives used are shown in Figure 1. All compounds have the same CTV crown-like core and differ only in their peripheral alkyl chains.

The CTV core is hexasubstituted with first-generation self-assembling (3,4)G1-CH<sub>2</sub> benzyl ether minidendrons. Each

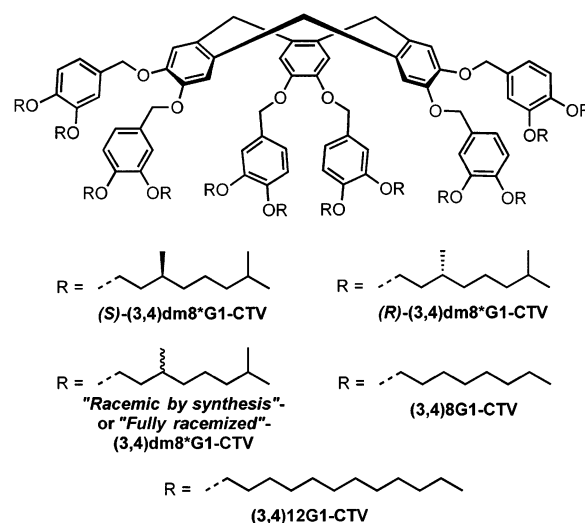


**Figure 1.** Structures of chiral and achiral dendronized cyclotrimeratrylene (CTV) derivatives.

dendron bears two peripheral alkyl chains, which can be either chiral branched chains ((*S*)- or (*R*)-3,7-dimethyloctyl (denoted *dm8\**)) or achiral linear chains (denoted 8 for  $-C_8H_{17}$  and 12 for  $-C_{12}H_{25}$ ). The synthesis and characterization of the compounds from Figure 1 are reported in the Supporting Information (Schemes SS1 and SS2). Their synthesis is based on reported procedures.<sup>13a,14</sup> Preparation of the (3,4)G1-CO<sub>2</sub>CH<sub>3</sub> dendron consisted of the alkylation of methyl 3,4-dihydroxybenzoate using the appropriate bromoalkanes (3,7-dimethyloctyl bromide, 1-bromooctane, or 1-bromododecane). Reduction of the ester to give the benzyl alcohol and subsequent reaction with thionyl chloride yielded the benzyl chloride (Scheme SS1, Supporting Information). In the final step of the synthesis six dendrons were attached to the demethylated CTV derivative CTV(OH)<sub>6</sub> to form the target dendronized CTV (Scheme SS2, Supporting Information). The pure enantiomers, (*S*)-(3,4)*dm8\**G1-CTV and (*R*)-(3,4)-*dm8\**G1-CTV, were obtained following this synthetic method, starting from the enantiopure branched bromoalkanes (*S*)-3,7-dimethyloctyl bromide and (*R*)-3,7-dimethyloctyl bromide, respectively. The compound, named "fully racemized-(3,4)-*dm8\**G1-CTV", "an irreversible racemized CTV", also referred in the rest of this report as "racemic by synthesis", was obtained by synthesis with the racemic 3,7-dimethyloctyl bromide. This compound is not a single chemical species but rather a mixture of stereoisomers. In the first alkylation step of this synthesis four distinct stereoisomers ((3*S*,4*S*), (3*S*,4*R*), (3*R*,4*S*), and (3*R*,4*R*), respectively) are formed by statistical addition of *S* or *R* alkyl chains at the 3 and 4 positions of the benzyl ring. These stereoisomers were not separated, and therefore, the benzyl chloride derivative obtained is still a mixture of four stereoisomers. Statistical addition of these stereoisomers to each of the six positions of the CTV core in the final synthetic step gives rise to an increased number of stereoisomers in the final product. Thus, the racemic by synthesis-(3,4)*dm8\**G1-CTV is a mixture of stereoisomers where molecules have *S* and *R* stereogenic centers in random proportions and positions at their 12 peripheral alkyl chains. Besides compounds (*S*)-(3,4)*dm8\**G1-CTV, (*R*)-(3,4)*dm8\**G1-CTV, and racemic by synthesis-(3,4)*dm8\**G1-CTV depicted in Figure 1, additional samples were prepared by mixing the pure enantiomers (*S*)-(3,4)*dm8\**G1-CTV and (*R*)-(3,4)*dm8\**G1-CTV in various

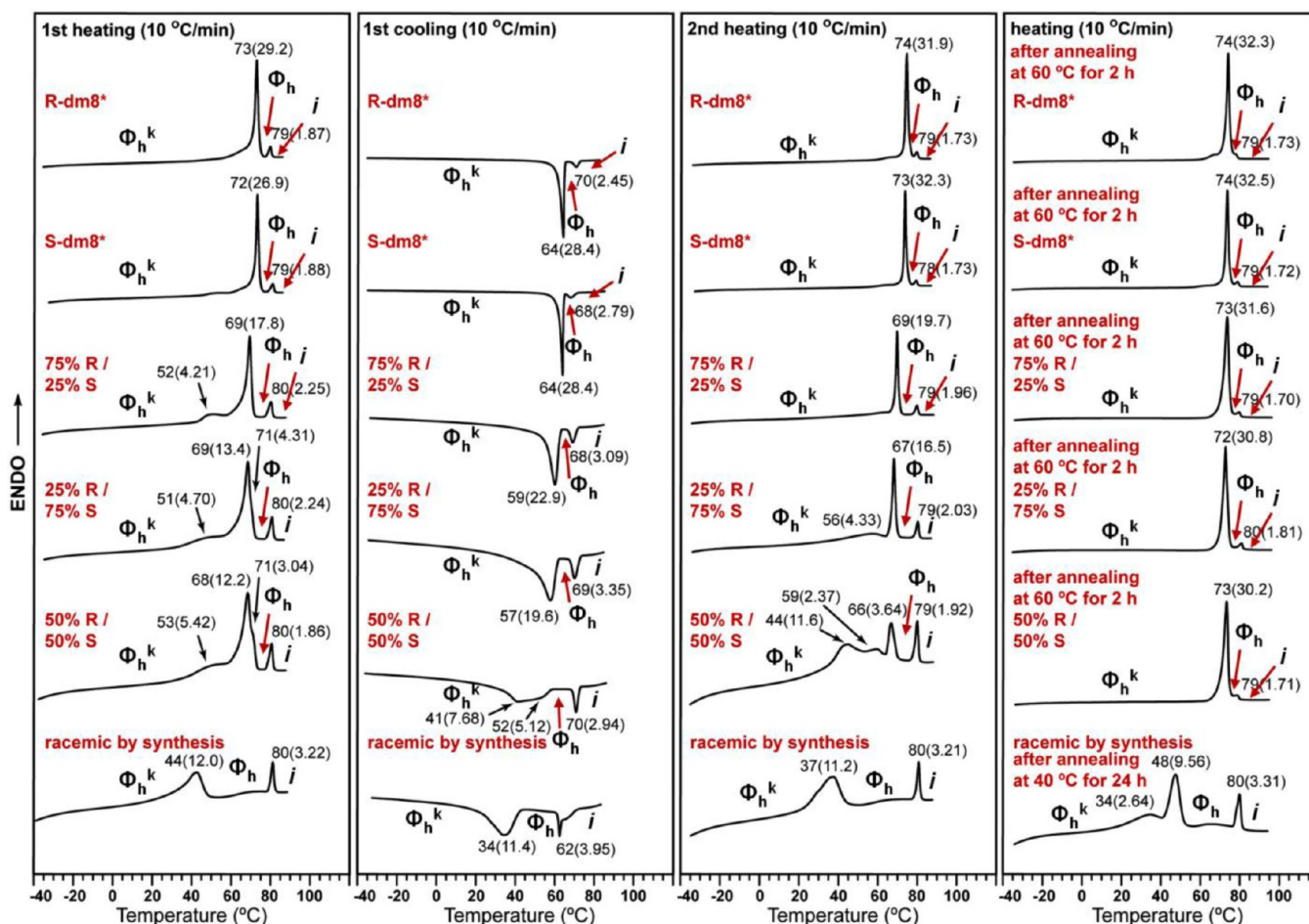


**Figure 2.** DSC traces of (*R*)- and (*S*)-(3,4)dm8\*G1-CTVs, of their mixtures with different compositions, and of the racemic by synthesis dendronized CTV recorded with heating and cooling rates of 10 °C/min. The right column shows the heating traces after annealing at the indicated temperature and time, cooling to  $-40$  °C, and reheating. Phases determined by XRD, transition temperatures, and associated enthalpy changes (in brackets in kcal/mol) are indicated ( $\Phi_h^k$  = columnar hexagonal crystal;  $\Phi_h$  = 2D columnar hexagonal liquid crystal; *i* = isotropic liquid).

ratios: 1:3, 3:1, and 1:1. The 1:1 mixture, also referred to as racemic by mixing, differs from the racemic by synthesis or fully racemized-(3,4)dm8\*G1-CTV described above. The racemic by mixing is a mixture of only two distinct chemical species that are enantiomers: (*S*)-(3,4)dm8\*G1-CTV (which contains only *S* chains) and (*R*)-(3,4)dm8\*G1-CTV (which contains only *R* chains). Since racemic by mixing and racemic by synthesis have very distinct compositions, they are expected to have different self-assembly behaviors. These differences will help us understand the role of chirality in the helical supramolecular polymerization of dendronized CTV derivatives. Finally, the achiral derivatives (3,4)8G1-CTV and (3,4)12G1-CTV were also synthesized following identical procedures to compare their self-assembly behavior with that of chiral dendronized CTV.

**Thermal Analysis of Chiral, Racemic, and Achiral Dendronized CTVs by Differential Scanning Calorimetry.** Figure 2 shows the differential scanning calorimetry (DSC) traces of the chiral enantiopure (*S*)- and (*R*)-(3,4)dm8\*G1-CTV, of their 75% (*S*)/25% (*R*), 25% (*S*)/75% (*R*), and 50% (*S*)/50% (*R*) mixtures, and of the fully racemized or racemic by synthesis CTV samples at heating and cooling rates of 10 °C/min. The sample with 50% (*S*)/50% (*R*) composition is the racemic by mixing.

The first three columns from the left part of Figure 2 show DSC traces collected during first heating, first cooling, and second heating scans, respectively. The right column provides heating data recorded after annealing at 60 °C for 2 h and at 40 °C for 24 h followed by cooling to  $-40$  °C.

The pure *R* or *S* enantiomers showed identical traces during first and second heating scans and during first cooling scan with two phase transitions at 74 or 73 °C and 79 or 78 °C, respectively. This difference is most probably due to the slightly lower enantiomeric purity of *S*. Analysis by X-ray diffraction (XRD to be discussed later) demonstrated a hexagonal crystalline phase ( $\Phi_h^k$ ) at temperatures below 73 °C and a 2D hexagonal liquid crystalline ( $\Phi_h$ ) phase in the small temperature region between the crystalline phase and the isotropic liquid (74 or 73 to 79 or 78 °C). After annealing at 60 °C in the crystal state (selection of this temperature will be discussed in the NMR section) for 2 h and cooling to  $-40$  °C, subsequent heating scans of enantiomerically pure *S* and *R* showed the same traces as that obtained during second heating, except that melting occurred at 74 °C and isotropization at 79 °C for both *R* and *S*, indicating that the annealing process did not further improve the order of the crystalline phase (right side column in Figure 2). By mixing the two enantiomers in a ratio of 75% (*S*)/25% (*R*) or 75% (*R*)/25% (*S*), the melting temperature of the crystalline phase decreased and a small new

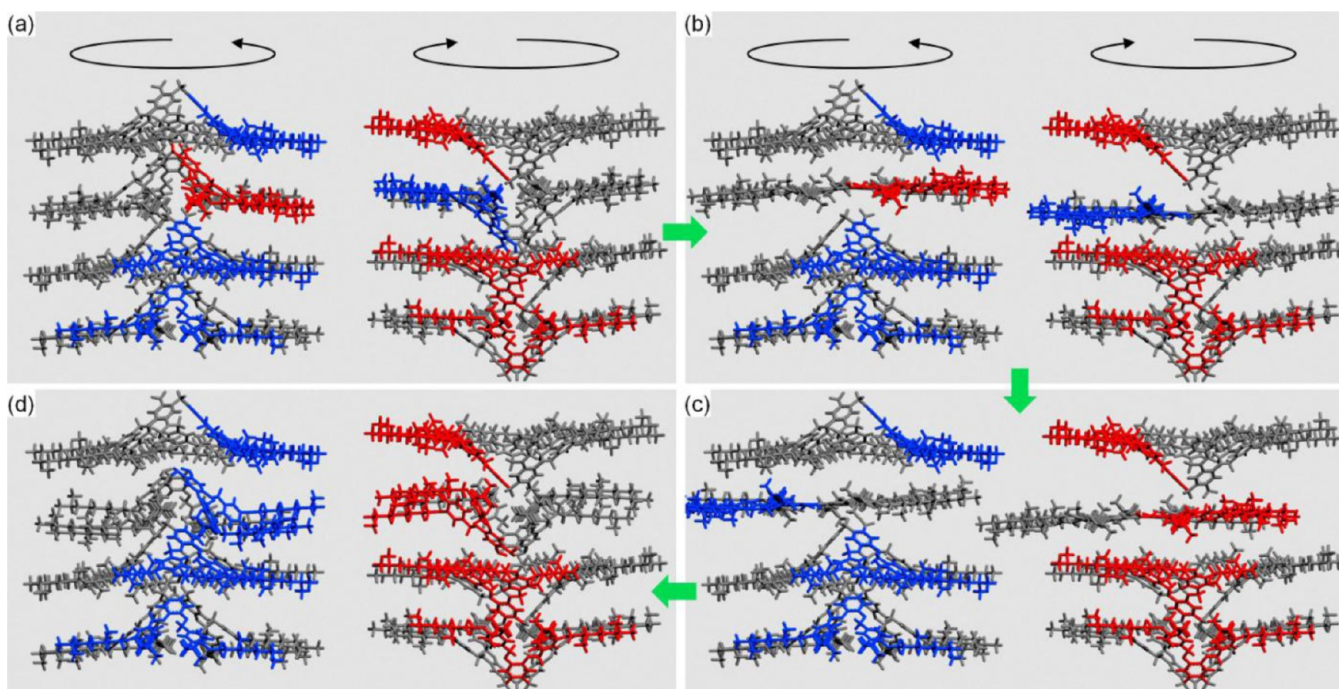
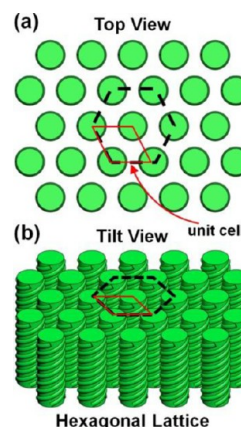


**Figure 3.** Sequence of events taking place during the deracemization process between enantiomerically rich columns assembled from the hat-shaped dendronized CTV (a) via a temporary disc-like conformation moving from column to column during the CTV crown inversion (b, c, d). A movie file is available in the Supporting Information.

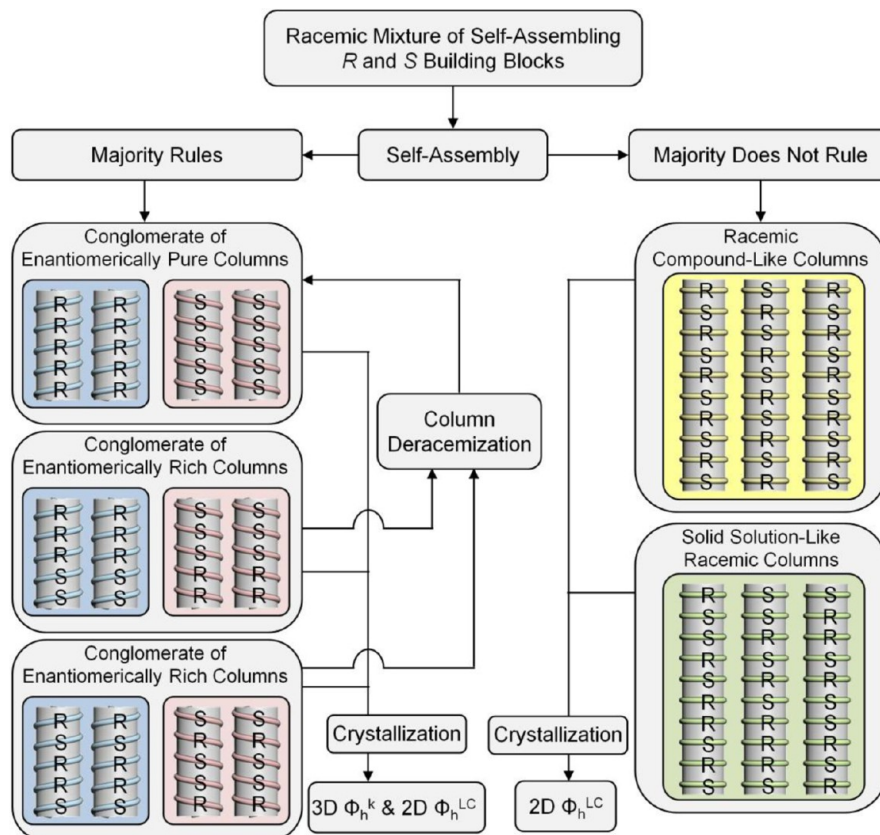
broad peak centered at about 52 °C appeared on the first heating scan. Nevertheless, the isotropization temperature remained the same, suggesting that the stability of the 2D  $\Phi_h$  periodic array is not affected by the enantiomeric composition of the mixture. A “majority-rules” experiment that will be discussed later demonstrated that in mixtures of 75% (*S*)/25% (*R*) and 75% (*R*)/25% (*S*) almost all supramolecular columns possess the same handedness as the enantiomerically pure columns. Therefore, the decrease in crystal melting temperature of the *R/S* mixtures is attributed to crystals generated from nonperfect columns with compositions ranging from enantiomerically pure to enantiomerically rich. Columns with identical handedness containing both enantiomers cannot establish a perfectly ordered intercolumnar correlation in  $\Phi_h^k$  and, therefore, form less ordered lower melting crystals dependent on the defect density in the columns. The stability of the 2D  $\Phi_h$  structure is not affected since it does not depend on the 3D correlation between columns. The same effect is even more clear with 50% (*S*)/50% (*R*). The melting peak of this crystalline phase splits into three broader peaks, which implies formation of crystal domains with different stabilities due to the inhomogeneous mixing of enantiomers. Interestingly, upon annealing at 60 °C for 2 h, cooling to −40 °C, and reheating, all mixtures (75% (*S*)/25% (*R*), 25% (*S*)/75% (*R*), and 50% (*S*)/50% (*R*)) showed again a single melting temperature that is identical to that of the pure enantiomers (compare the fourth and third columns in Figure 2). These results indicate a deracemization or spontaneous resolution of the columns containing different enantiomeric excesses that occurred during annealing at 60 °C in the  $\Phi_h^k$  phase for 2 h. This deracemization makes the columns become enantiomerically pure in order to enhance their crystal order. The deracemization process implies diffusion of molecules between columns at the annealing temperature. At 60 °C the crown conformation of CTV undergoes an umbrella-like inversion (to be discussed in

the NMR section); during its transient disc-like conformation, the dendronized CTV moves from column to column (Figure 3). A movie that includes the snapshots in Figure 3 is available in the Supporting Information.

This process was studied by solid state NMR and will be discussed in a different subsection. Annealing in the 2D  $\Phi_h$  phase does not induce deracemization since this spontaneous optical resolution or chiral self-sorting is driven by establishment of higher 3D intercolumnar order in the  $\Phi_h^k$  structure, which demands all columns to have the same handedness in a crystalline domain (Figure 4 and to be detailed in a later subsection). In the racemic by synthesis dendronized CTV *R* and *S* configurations are distributed randomly among the 12 side chains. The DSC curve of this sample shows only one



**Figure 4.** Schematic representation of columnar crystalline hexagonal lattice ( $\Phi_h^k$ ) with the unit cell (red box) indicated in (a) top view and (b) tilt view. Each unit cell contains one single column which implies single-helical handedness for all columns in the crystal.

Scheme 1. Crystallization of a Racemic Mixture of Self-Assembling R and S Building Blocks Forming Columnar Assemblies<sup>a</sup>

<sup>a</sup>Two sequences of R and S enantiomers are shown for conglomerates of enantiomerically rich columns (bottom and middle left side).

broad crystal melting peak at lower temperature (37 °C) upon second heating. This transition corresponds to the melting of low-ordered crystals created by the poor packing of columns generated from the two enantiomers. After annealing at 40 °C for 24 h, only a fraction of crystals increased their melting temperature to 48 °C, suggesting that after an extended period of annealing in the crystalline phase the racemic by synthesis sample cannot improve the crystal order to the same extent as that observed in pure enantiomers. This indicates that it is not possible to achieve perfect 3D column to column correlation in  $\Phi_h^k$  if complete deracemization of CTV enantiomers is not accessible at the molecular level. Even in this case, all columns from the crystal domain must have overall the same handedness with reverse rotation sense molecules as defects (see below the discussion of XRD and CD). In summary, the difference in phase stability and crystallization behavior is greatly affected by the enantiomeric composition within columns. The pure R or S enantiomers tend to stack into columns with selected handedness, and columns with the same handedness and molecular chirality can pack with each other three dimensionally with long-range order to form stable  $\Phi_h^k$  crystals possessing a high melting temperature. The  $\Phi_h^k$  phase consisting of monodomains of left- or right-handed supramolecular columns formed from various ratios of CTV enantiomers resemble low molar mass conglomerates, albeit produced according to more complex principles (compare Scheme 1 and Scheme SS3, Supporting Information).<sup>3b</sup>

**X-ray Fiber Diffraction and Molecular Models of the Supramolecular Columns from Enantiopure (3,4)-dm8\*G1-CTV and from Achiral (3,4)8G1-CTV Com-**

**pounds.** The fiber diffraction pattern of the R enantiomer of (3,4)dm8\*G1-CTV is shown in Figure 5m, and that of its achiral or nonchiral analogue with linear pendant chains, (3,4)8G1-CTV, is shown in Figure 6. Both are in the crystalline  $\Phi_h^k$  phase. The 3D order is evident in both patterns by the presence of discrete Bragg reflections on a number of layer lines. The observed indexed Bragg spacings are listed in Table ST2, Supporting Information.

The *c* axis is along the column axis which is also parallel to the fiber direction. All samples show sharp equatorial (*hk*0) reflections corresponding to a well-ordered hexagonal array. The numerous strong and sharp (*hkl*) reflections observed for pure enantiomers (Figures 5m, 7a, and 7d) indicate a long-range ordered crystal structure ( $\Phi_h^k$ ) with highly correlated molecular positions between neighboring columns. The four layer lines perpendicular to the fiber axis would suggest a  $4_1$  helical columnar structure. As the molecule itself has 3-fold  $C_{3v}$  symmetry, it would be more appropriate to view the column as a  $12_1$  triple helix or a  $12_3$  helix. Note that a +90° rotation between successive  $C_{3v}$  molecules, implied by a right 4-fold helix, is equivalent to a -30° rotation of a left 12-fold helix. However, we note that the above refers only to isolated columns. Once put in a periodic hexagonal 3D lattice, the  $4_1$  or  $12_3$  symmetries become only approximations, as they are incompatible with any hexagonal space group.

The hexagonal unit cell parameters for the two enantiomers of (3,4)dm8\*G1-CTV are  $a = 34.3$  Å (the "column diameter") and  $c = 18.5$  Å. The distance between two molecules along the column axis is 4.6 Å (the *d* spacing of the (004) reflection), and the pitch (full turn) of the 12-fold helix is 55.5 Å. That there are

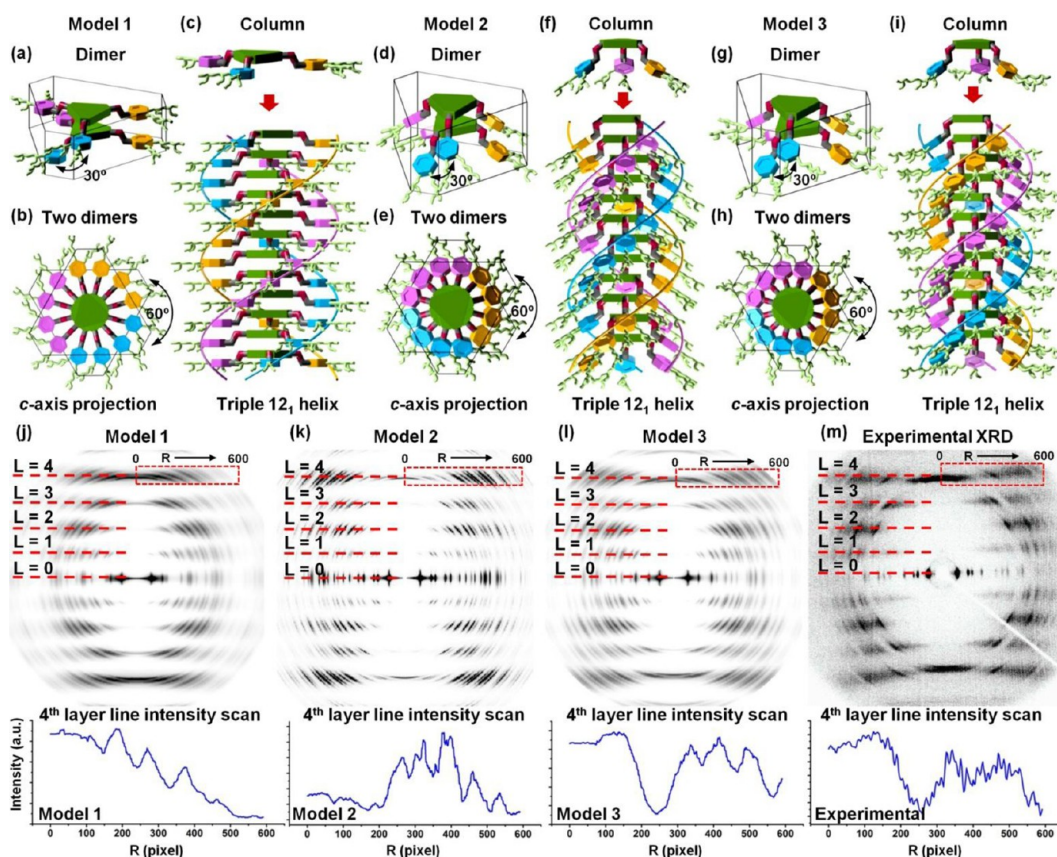


**Figure 5.** Schematic models of (a, d, g) two successive CTV molecules within a column, (b, e, h) packing of two dimers viewed along the  $c$  axis, and (c, f, i) supramolecular column with approximate triple  $12_1$  helix conformation and  $P6_3$  crystal symmetry for the three models with different side chain orientations. Comparison of the simulated fiber XRD patterns from model 1 (j), model 2 (k), and model 3 hat-shaped (l) with the experimental pattern (m) of the 3D  $\Phi_h^k$  crystalline phase of the  $R$  enantiomer of (3,4)dm8\*G1-CTV. The fourth layer line intensity scans obtained in the red box region are shown at the bottom.

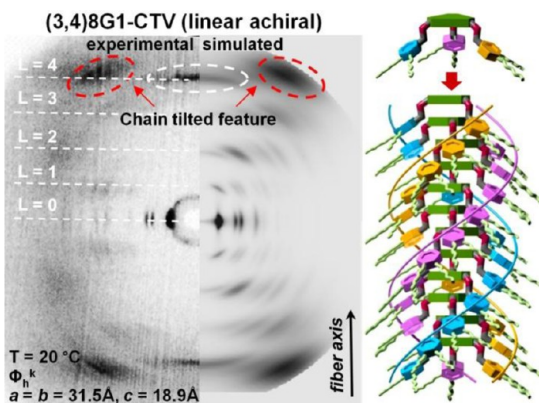


**Figure 6.** Comparison of the experimental and simulated fiber XRD patterns of (3,4)8G1-CTV. Column model used in the simulation is shown on the right.

4 molecules per unit cell has been confirmed by the comparison of unit cell volume and experimental density ( $1.04 \text{ g/cm}^3$ ) (Table ST3, Supporting Information). There is only one column per unit cell. The columns are thus assembled by the stacking of CTV cores with one molecule per column stratum of  $4.6 \text{ \AA}$ . With the absence of meridional  $00l$  reflections with  $l = \text{odd}$  and with no other systematic extinctions there are three possible space groups:  $P6_3$ ,  $P6_3/m$ , or  $P6_322$ . However, since the molecules do not possess either a mirror plane or a 2-fold

axis normal to the 3-fold axis, only the  $P6_3$  space group (space group no. 173) remains. The possibility that these additional lattice symmetry elements may be present due to random inversions of the “hat-shaped dendronized CTV” is not excluded, since “hat inversions” do not racemize the system, as shown by circular dichroism (see below). Therefore, the  $P6_322$  space group is less probable.

Since the  $\Phi_h^k$  unit cell contains a single column the above implies that all 4 molecules in the cell and all columns in the crystal domain possess the same helical sense (Figure 4).<sup>15</sup>

As already noted, strict  $12_3$  or  $4_1$  screw axis symmetry is incompatible with hexagonal crystal symmetry. The true crystallographic symmetry is  $6_3$ , or triple  $2_1$ , and takes account of the column environment, not just the column itself. Thus, the asymmetric unit is in fact a dimer (Figure 5a, 5d, and 5g), the unit cell containing two dimers related to each other by a  $2_1$  operation. The two molecules in the dimer are not mutually related by crystal symmetry but are similar and related *approximately* by the  $4_1$  or  $12_3$  symmetry, i.e., by a  $90^\circ$  or  $30^\circ$  rotation. A second dimer is seated on top of the first one, rotated by  $180^\circ$  ( $2_1$ ) or  $60^\circ$  ( $6_3$ ) relative to the first dimer, and moved up by one-half of the  $\Phi_h^k$  unit cell along the  $c$  axis to generate a continuous helix with intermolecular rotation of  $30^\circ$  (Figure 5b, 5e, and 5h). The absence of the  $002$  reflection is thus not a systematic absence, as the space group allows it. This is a common situation, and  $00l$  reflections forbidden by the *apparent* helical symmetry of the column are often observed.<sup>10c,d</sup> Their intensity reflects the degree of distortion that

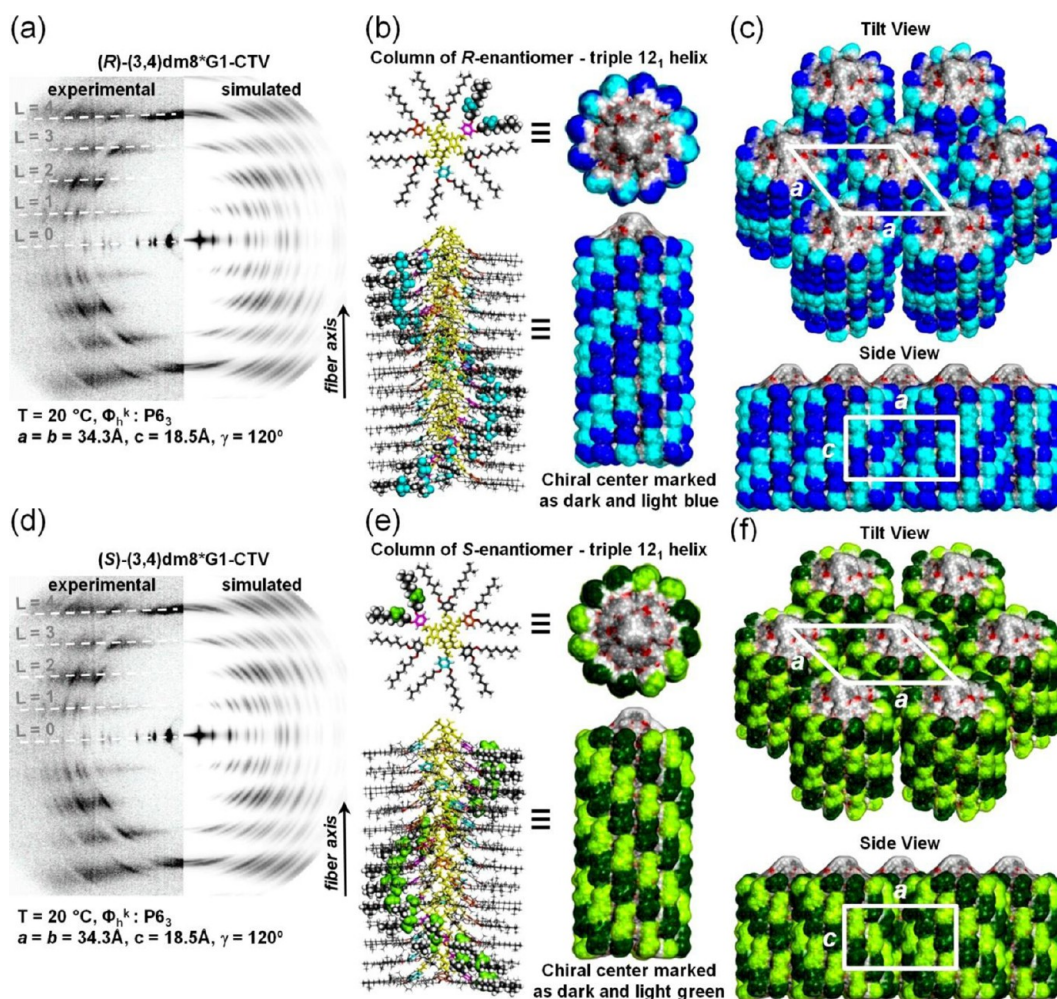


**Figure 7.** Comparison of the experimental and simulated fiber XRD patterns of the  $\Phi_h^k$  3D crystalline phase of the (a) *R* and (d) *S* enantiomers. Models of the supramolecular columns seen from the top and side views constructed by the (b) *R* and (e) *S* enantiomers. The helical sense was determined by CD-UV experiments. Chiral centers are decorated as dark/light blue for the *R* enantiomer and dark/light green for the *S* enantiomer for easy visualization of the helical structure. Crystal packing models for top and side views of the (c) *R* and (f) *S* enantiomers in the  $\Phi_h^k$  lattice. In both models combinations of up and down columns are allowed by the hat-shaped dendronized CTV (see also Figure SF10b, Supporting Information).

crystal packing exerts on the columnar helix. The resulting supramolecular column is depicted in Figure 5c, 5f, and 5i as discussed below.

We proceeded to build detailed molecular models and fit the experimental diffraction pattern to those simulated from the models. Figure 5 outlines possible molecular models of the supramolecular columns forming a  $\Phi_h^k$  periodic array. Simulations of their fiber XRD patterns and comparison with the experimental data are also shown. Three models with identical helical conformation of the CTV columnar core but with different side chain conformations/orientations were considered. In model 1, the benzyl ether and alkyl chains are perpendicular to the column, whereas they are all tilted in model 2. In model 3, the benzyl ether is tilted and the alkyl chains start tilting near the junction point of the dendron but ultimately become perpendicular to the long axis of the column. This arrangement provides an unprecedented “hat-shaped” dendronized CTV conformation. Simulated fiber XRD patterns obtained from  $\Phi_h^k$  arrays generated from each model are shown in Figure 5j, 5k, and 5l, respectively.

The most significant differences between these patterns are the intensity distributions along the  $L = 4$  layer line, which are

affected mostly by the orientation of the dendron and its alkyl groups (bottom plots of Figure 5j, 5k, and 5l). When we compare the simulated and experimental fourth layer line scans, it becomes clear that model 3 based on the hat-shaped dendronized CTV best agrees with the data. In model 3 the chains are straight and tilted near the junctions with the benzene rings but become horizontal toward the chain ends. This suggests that as moving toward the chain ends in the chiral compounds, the branching and increased conformational disorder (likelihood of gauche bonds) increase the effective chain cross-section and lead to their horizontal conformation. Model 2 from Figure 5f requires an up–down alternation between the pine-tree columns (antiparallel) in the  $\Phi_h^k$  phase to ensure effective packing between the alkyl groups. This arrangement would require two columns per unit cell and thus reduce the hexagonal symmetry of the 3D  $\Phi_h^k$  periodic array to orthorhombic or monoclinic.<sup>10b–d</sup> This arrangement is not demanded by the bent-branch pine-tree columns generated from the hat-shaped dendronized CTV (model 3 in Figure 5i) since the packing of the alkyl group in adjacent columns does not depend on the up or down orientation of the columns (for comparison of the two column packing models 2 and 3 see

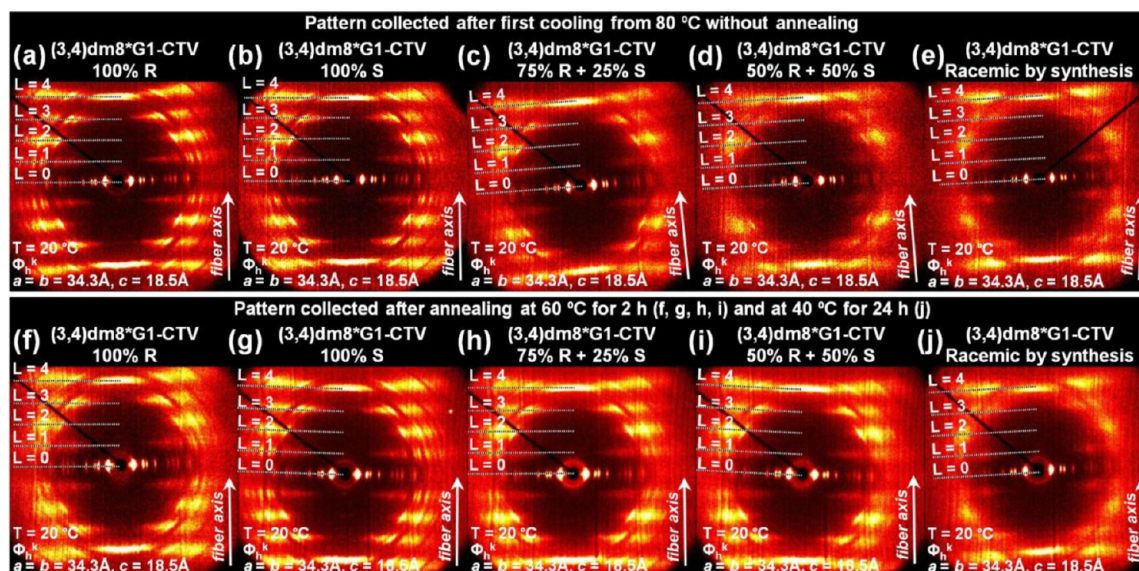


**Figure 8.** Wide angle X-ray diffraction patterns collected from the oriented fibers of chiral CTVs with indicated composition. (a–e) Patterns collected at 20 °C after first cooling from 80 to 20 °C with a rate of 10 °C/min without annealing. (f–i) Patterns collected at 20 °C after annealing at 60 °C for 2 h and cooling to 20 °C with a rate of 10 °C/min, and (j) annealing at 40 °C for 24 h and cooling to 20 °C with a rate of 10 °C/min. Fiber axis, layer lines (L), temperature, phase, and lattice parameters are indicated.

Figure SF10, Supporting Information). Conversely, for the columns with linear achiral side groups the chains are more tilted (closer to model 2 in Figure 5k) as their effective cross-section is narrower. A diffraction feature associated with the chain tilt can be readily identified in both the simulated and the experimental patterns of (3,4)8G1-CTV (red oval in Figure 6). However, the weaker meridian reflection in the simulated pattern (white oval) implies that toward the chain ends the linear alkyl chains curve toward a horizontal orientation, although not as much as in the case of the branched chiral chains. This behavior is understandable as the probability of the gauche conformation increases toward the chain end in both cases, but the extra space required by the branch is not required in (3,4)8G1-CTV.

Evidence for increased gauche conformation toward chain ends in *n*-alkanes is well documented in the literature<sup>16</sup> and confirmed by <sup>13</sup>C solid state NMR measurements for (3,4)8G1-CTV (Figure SF9, Supporting Information). The (3,4)8G1-CTV with linear side chains showed blurred layer lines in the XRD pattern, indicating a helical structure with poor long-range crystal order despite a well-defined local packing observed in solid state NMR measurements (Figure SF9, Supporting Information). The first and second layer lines in the simulated pattern have their maxima closer to meridian than those in the experimental XRD, indicating that the actual helical structure is narrower than in the molecular model. This is most likely because the disordered outer parts of the alkyl chains contribute only to isotropic diffuse scattering and, therefore, give a narrower helix and a wider cross. A similar situation is seen in the diffraction pattern of the DNA helix where the cross-pattern is narrower in the simulated pattern than in the experimental one.<sup>17</sup> It may be speculated that the reason for lower intercolumnar order in the linear-chain (3,4)8G1-CTV compound compared to that in the branched (3,4)dm8\*G1-CTV is the fact that the tilted chains of the former are more difficult to interdigitate than the horizontal chains of the latter (Figure SF10, Supporting Information). Effective interdigitation is believed to promote intercolumnar positional correlation

and disregard the up and down arrangement of adjacent columns.

In contrast, the structure generated by mixing chiral and linear CTV compounds loses the tilted chain feature and displays no crystal order (Figure SF2, Supporting Information), indicating that mixing inhibits the preferred alkyl chain conformation for each compound and thus makes it difficult to establish crystal order between neighboring columns (Figure 4).

The supramolecular columnar structures, crystal models, and comparison between simulated and experimental fiber XRD patterns of the  $\Phi_h^k$  structure for the two enantiomers are shown in Figure 7. The simulated diffraction patterns based on the molecular models constructed with the cell symmetry discussed above are shown in Figure 7a and 7d for the *R* and *S* enantiomers, respectively. The helical sense of the *R*- and *S*-based models was determined by CD-UV experiments to be discussed in a different subsection. Very good agreement between the experimental and the simulated patterns is observed. In the columnar model shown in Figure 7b and 7e the left side shows the hat-shaped dendronized CTV single molecule and the columnar model with the chiral centers highlighted. The  $12_1$  helical structure and the relative positions of the chiral center in the right- or left-handed columns can be easily identified. The right side shows the columnar model with the potential surface. For clarity, the alkyl chain segments after the chiral center were cut off. The chiral centers, marked with dark and light blue for *R* enantiomers and dark and light green for *S* enantiomers, show the triple helix structures with opposite handedness. Tilted and side views of a model containing 7 enantiomerically pure columns are shown in Figure 7c and 7f. A hexagonal unit cell is labeled by the white boxes. Only one column can be accommodated in the unit cell, indicating that all columns in the crystal are required to possess the same handedness (see  $\Phi_h^k$  unit cell in Figures 4 and 7c). The high degree of intercolumnar correlation of molecular positions can be identified from the side view of the unit cell models that result in a long-range ordered 3D periodic array.

### Comparison of Chiral Assemblies of Enantiopure *R*, *S*, and Various Enantiomeric Ratios Including “Racemic by Mixture” and Racemic by Synthesis by Fiber XRD.

The top row in Figure 8 shows the XRD patterns collected at 20 °C from the  $\Phi_h^k$  phase obtained from pure CTV enantiomers, various mixtures of enantiomers, and racemic by synthesis CTV collected from oriented fibers after first cooling from 80 to 20 °C. When two enantiomers were mixed with a 75% (*S*)/25% (*R*) or 75% (*R*)/25% (*S*) ratio (Figure 8c), the degree of intracolumnar order and column–column correlation decreased. This is seen from the general broadening of the Bragg reflections but most conspicuously from the weakening of the odd layer lines ( $L = 1, 3$ ). One should appreciate that 18.5 Å ( $4 \times 4.6$ ) periodicity (first layer line) comes from the 4 successive molecules twisting in the same direction by 90°. If that was not the case and the rotation was alternatively by +90° and –90°, the period would have been only 9.2 Å (2nd layer line) and the odd layer lines would have not existed.

A simulation of the XRD pattern of the  $\Phi_h^k$  phase generated from nonhelical columns (Figure 9) demonstrated the absence

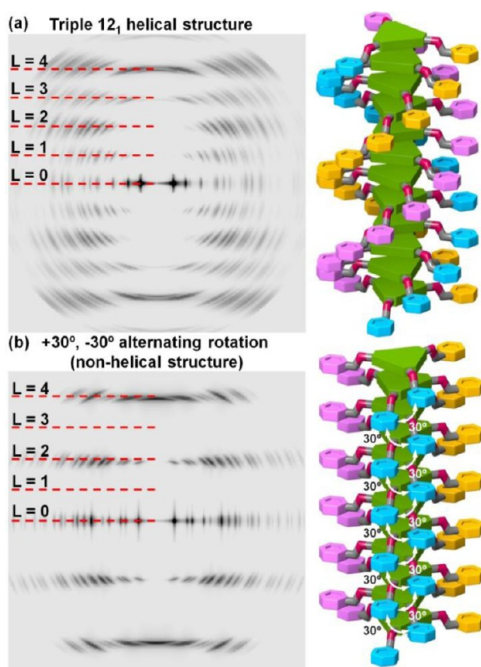


**Figure 9.** Simulated fiber crystal XRD pattern and the corresponding schematic columnar structure for (a) triple  $12_1$  helical structure and (b) nonhelical structure generated by alternating +30°, –30° rotation of molecules along column. Loss of odd layer lines is evident in the nonhelical structure.

of Bragg reflections at  $L = 1$  and 3. Similar disappearance of odd layer lines is expected if the sequence of positive and negative molecular rotations was random. It is thus understandable that a mixture with a considerable amount of opposite enantiomer disrupts the sense of intermolecular twist and thus weakens the odd layer lines disproportionately. These results are consistent with the DSC analysis, which suggests that less than 100% enantiomeric purity results in non-enantiopure columns or even in columns with opposite handedness that are incompatible with the  $\Phi_h^k$  unit cell requirement of single handedness column, leading to poor intercolumnar correlations. With a 50% (*R*)/50% (*S*) mixture (Figure 8d) the overall 3D crystal order is further reduced in

the as-prepared sample, and only a few off-meridional reflections were observed, suggesting that a large portion of columns is constructed with random mixtures of enantiomers (Scheme 1), further hindering correlations between the neighboring columns of the  $\Phi_h^k$  phase. The weaker odd layer lines in the pattern also suggest that the columns may undergo very frequent helix reversals as defects in the homochiral  $\Phi_h^k$  crystal domain.

Even less crystal order was observed in the racemic by synthesis 3D columnar periodic array (Figure 8e) where columns are made of molecules with totally random side chain chirality. The low-order and inhomogeneous crystal structure gives lower and less defined melting temperatures (Figure 2). Nevertheless, all samples exhibit a sharp and strong 4.6 Å meridian reflection that indicates a well-defined CTV to CTV distance of 4.6 Å. This is not surprising because this is the one feature that is totally independent of the stereochemistry from the side groups of the dendronized CTV. In other words, the crown stacking periodicity is not influenced by their side chain chirality.

The bottom row in Figure 8 shows the XRD patterns obtained for each top sample after annealing at 60 °C for 2 h (compare Figure 8a–d with 8f–i) or annealing at 40 °C for 24 h (Figure 8j) where fast motion was observed by solid state NMR (to be discussed in a later section). No marked improvement is seen in the crystalline order of the pure enantiomers (Figure 8f and 8g), as the order had already been high before annealing. It is very telling, however, that the crystal order of the mixtures of enantiomers was improved greatly (Figure 8h and 8i). In particular, the pronounced strengthening of the  $L = 1$  and 3 layer line reflections after annealing (compare Figure 8a–d with 8f–i) shows that even in random enantiomeric mixtures, including the 50% (*S*)/50% (*R*) blend, coherent crystal domains of considerable size are formed consisting of single-handed helical columns since the XRD patterns became similar to those recorded from enantiomerically pure columnar structures.

Therefore, these results demonstrate deracemization of enantiomers and phase separation of helical columns with monodomains of left- and right-handed columns forming  $\Phi_h^k$  during the annealing process. However, only a slight improvement of crystal order was identified for the racemic by synthesis compound even after annealing for 24 h (Figure 8) (since in this case the random distribution of *R* and *S* chains within monomers cannot drive a complete phase separation of enantiomerically pure columns). Similarly, the annealing treatment does not improve the  $\Phi_h^k$  order for columnar arrays generated from achiral compounds with linear chains or mixtures of chiral and achiral molecules (Figure SF3, Supporting Information). It is interesting to note that, similarly, it has been reported that enantiopure helicene molecules also form large single-handed 3D hexagonal arrays. In their racemic mixture the two enantiomers form their separate left- and right-handed helical columns, but in that case both column types cocrystallize forming a regular alternating array, in this case monoclinic.<sup>15</sup>

**Analysis of the Molecular Dynamics of the Supramolecular Columns Produced from Racemic by Synthesis and Enantiopure *S* by Variable-Temperature Solid State <sup>13</sup>C NMR Experiments.** Solid state NMR experiments can provide unique information about the time scale and, due to its site selectivity, the mechanism of molecular motions of the building blocks.<sup>18</sup> Such motions must take place

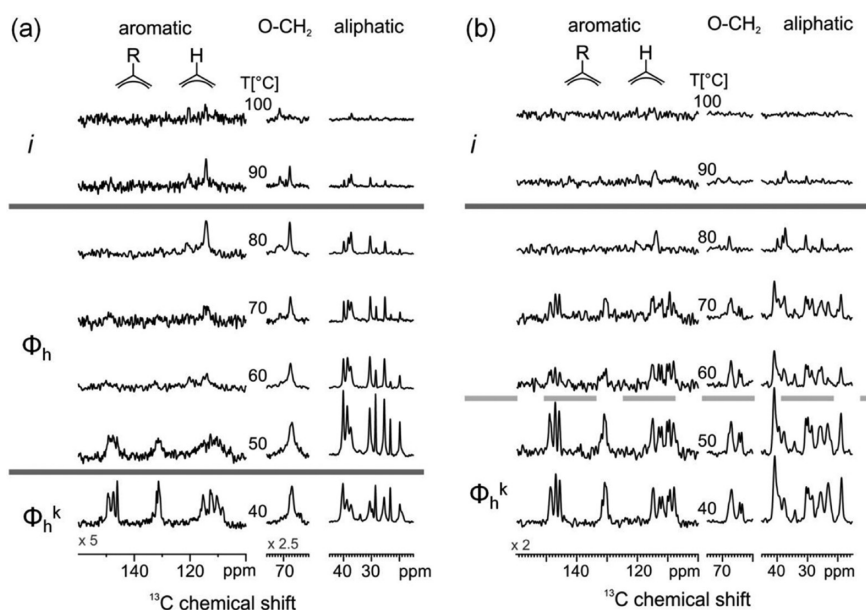


**Figure 10.** Temperature-dependent  $^{13}\text{C}$  CP-MAS NMR spectra of (a) racemic by synthesis dendronized CTV and (b) (S)-(3,4)dm8\*G1-CTV, recorded at 700 MHz  $^1\text{H}$  Larmor and 25 kHz MAS spinning frequency. Different spectral regions are plotted on different intensity scales, as indicated.

if the supramolecular columns are to reorganize, as discussed in the earlier DSC and XRD analysis sections. The dynamic processes can be most easily studied in the racemic by synthesis CTV sample because of the broad LC phase it exhibits (Figure 2). Moreover, the wealth of information that exists about molecular motions in columnar discotic LCs<sup>19</sup> can be employed in our analysis. The most prominent molecular motions in 2D columnar structures are rotations about the column axis. A recent study combining XRD, dielectric spectroscopy, and solid state NMR is available.<sup>20</sup> Moreover, complex dynamic processes have been identified, where moieties forming columnar structures leave the column, flip over, and return to the columns again.<sup>10b</sup> Early work on translational diffusion of disc-like molecules revealed that diffusion between the columns is much faster than motion along the column.<sup>21</sup> This means that in columns assembled from disc-like molecules rotation of discs that are most easy to detect by solid state NMR are intimately linked to processes that allow reorganization of the columnar structures.

Indeed, well-established  $^{13}\text{C}$  cross-polarization (CP) MAS NMR data already provide a wealth of information. Spectra are well resolved in well-ordered crystalline states but also in highly mobile LC systems. The signals severely lose intensity for moieties involved in motions on the tens of kHz time scale due to interference effects of the fluctuating dipole–dipole couplings with the radiofrequency pulses and the MAS rotation frequency, which can be used to assign molecular motions to specific sites in complex systems.<sup>22</sup> The signals eventually vanish for rapid isotropic motions in the isotropic liquid.<sup>18</sup>

NMR spectra of the racemic by synthesis dendronized CTV sample (Figure 10a) and of the enantiopure sample (Figure 10b) show well-resolved spectra in the solid state at 40 °C, where all aromatic sites in the CTV unit are resolved. As indicated, they are grouped as quaternary carbons (130–150 ppm) and aromatic CH groups (110–120 ppm). In the  $\Phi_h$  LC phase at 50 °C (Figure 10a), the aromatic signals broaden (indicating kHz motions) whereas the aliphatic side groups become better resolved, indicating rapid anisotropic motions in

the 100 kHz to MHz range. At even higher temperatures, these signals become weaker as the increasing mobility averages the dipole–dipole coupling to the carbons, which are needed to generate signals via CP. Note that at 90 °C, i.e., in the molten state, small signals of the aliphatic carbons as well as those of aromatics are still detected. This indicates that columnar aggregates are still present at this temperature.

Remarkably, a signal due to an aromatic group at about 117 ppm “reappears” at higher temperatures (80–90 °C). It is assigned to the 6 chemically equivalent proton-carrying aromatic carbon sites in the crown. The signal of the  $\text{CH}_2$  groups of the CTV crown at 33 ppm, however, is completely gone. This indicates that the crown fluctuates between its “up” and “down” conformations. These conformational changes cause the  $^{13}\text{C}$ – $^1\text{H}$  dipole–dipole coupling to fluctuate strongly for all positions, except for these proton-carrying aromatic carbons, for which the C–H bond directions are close to the plane of the fluctuating crown. Thus, on average, the crown behaves like a disc at 50 °C for the racemic by synthesis (Figure 10a) and at 60 °C for the enantiopure (Figure 10b). As stated above, the prominent motions in LCs self-organized from disc-like molecules are the axial rotation about the column axis and the translation between columns. Therefore, we ascribe the pronounced dynamics detected in the CTVs by NMR to fluctuations in the columns and exchange between columns, which offers a mechanism for the deracemization observed in those range of temperatures both by DSC (Figure 2) and XRD (Figure 8) experiments. It should be noted that the time scales of the local motions detected here are in the range of tens of kHz, whereas deracemization occurs on a time scale of hours. This indicates that the building blocks forming the columnar structures need a large number of motional steps before equilibrium is reached. This is similar to the transition from disordered columns of dendronized perylene bisimides to their thermodynamically controlled state.<sup>10b</sup>

**Analysis of the Helical Supramolecular Polymerization by Circular Dichroism (CD) and UV Absorption Experiments in Solution and in Thin Film.** CD and UV

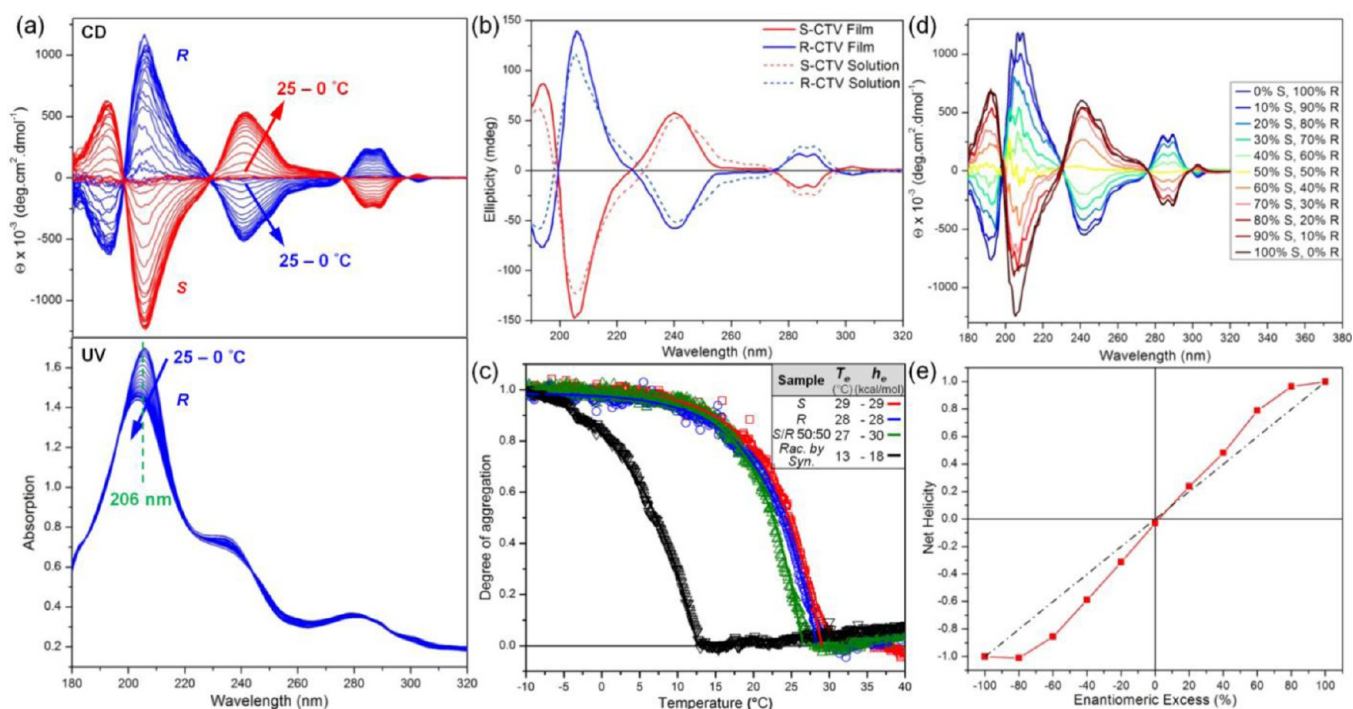


**Figure 11.** (a) CD and UV spectra of (S)- and (R)-(3,4)dm8\*G1-CTV upon cooling from 25 to 0 °C ( $4.0 \times 10^{-5}$  M in dodecane). S enantiomer is in red; R enantiomer is in blue. (b) Thin film CD spectra of S (red bold line) and R (blue bold line) enantiomer at 25 °C. Solution spectra (0 °C) are also given for comparison (dashed lines,  $4.0 \times 10^{-5}$  M dodecane solutions multiplied by a factor of 2.5). (c) Degree of aggregation (from UV absorption at 206 nm) collected upon cooling of *n*-butanol solutions from 50 to -10 °C (total concentration of dendrimers:  $4.0 \times 10^{-5}$  M for the S, R, and racemic by synthesis sample;  $8.0 \times 10^{-5}$  M for the S/R 50:50 sample), and fitting with the cooperative elongation model (solid lines). (d, e) Majority-rules experiment. (d) CD spectra collected from mixtures of two enantiomers at 0 °C in dodecane. (e) Net helicity dependence of the enantiomeric excess (from the ellipticity at 289 nm).

spectra of the pure enantiomers of (3,4)dm8\*G1-CTV in  $4.0 \times 10^{-5}$  M dodecane solution upon cooling from 25 to 0 °C are depicted in Figure 11a. Helical supramolecular polymerization in this solvent is evidenced by the emergence of a bisignated CD signal upon cooling. Dodecane was chosen as a solvent for this experiment because it promotes helical self-assembly of the dendronized CTV.<sup>13a,14</sup> At high temperatures the dendronized CTVs are molecularly dissolved, and no ellipticity is observed in the CD spectrum since the chiral centers are located in the peripheral alkyl chains which do not absorb in the UV region. However, upon cooling to lower temperatures, helical supramolecular polymerization occurs and chirality is transferred from the branched side chains to the central aromatic core of the molecular and supramolecular structure. Growth of the self-assembled columns upon cooling is reflected by the emergence of Cotton effects with increasing ellipticity in the CD spectra. The stereochemistry of the peripheral alkyl chains dictates the helical sense of the columns, as evidenced by the mirror image CD spectra obtained for the S and R enantiomers of (3,4)dm8\*G1-CTV (Figure 11a). While the helix handedness of the (S)-(3,4)dm8\*G1-CTV self-assembly is clearly the opposite of the handedness of the (R)-(3,4)dm8\*G1-CTV self-assembled helices, their absolute helical sense is more difficult to determine. Several contributions are overlapping in the CD spectra. However, the first couplet—with a peak at 193 nm and a trough at 206 nm for the S enantiomer—is a negative exciton coupling that corresponds to the main absorption band in the UV spectrum. According to the exciton coupling theory, this negative exciton coupling suggests that the S enantiomer of (3,4)dm8\*G1-CTV forms left-handed helical columns.<sup>23</sup>

Conversely, the self-assembled columns formed by the R enantiomer can be assigned as right-handed helical columns.

CD spectra of the enantiomerically pure (3,4)dm8\*G1-CTV were also recorded in the solid state. Thin films were cast on quartz plates by spin coating from 2% w/v chloroform solutions of the dendronized CTV. CD spectra in thin films are nearly identical to the spectra in solution (Figure 11b). This equivalence of the spectra in thin film and in solution confirms that very similar and shape-persistent self-assembled structures form both in the  $\Phi_h^k$  crystal state and in solution. Since CD spectroscopy is very sensitive to conformational changes, the high similarity of the spectra confirms that the dendronized CTV molecules adopt comparable conformations in their self-assembled state in the bulk state and in solution. The sign of the Cotton effects is also identical in thin film and in solution for a given enantiomer, which demonstrates that the helices have the same handedness in the solid state and in solution. This thin film CD experiment allows us to compare the helical columns determined by XRD in the solid state with the self-assembled structures analyzed by CD/UV spectroscopies in solution.

Self-assembly of the enantiomerically pure CTV in solution is reflected not only by the emergence of Cotton effects upon cooling but also by a slight blue shift and significant decrease of the intensity of the main UV absorption band at 206 nm. These changes in the UV spectra enable us to monitor the self-assembly process even in the case of racemic or achiral CTV dendrimers and to compare it with the self-assembly of enantiomerically pure (3,4)dm8\*G1-CTV. For racemic and achiral dendronized CTV no Cotton effect is observed upon cooling, either because the columns are not helical, or because

the columns contain equal proportions of right-handed and left-handed helical fragments whose CD contributions cancel each other, or because the columns are helical but exist in an equal ratio of right- and left-handed columns (Figure SF5, Supporting Information). Formation of racemic helical columns from a racemic dendrimer could result from two distinct processes. The first process would be a complete deracemization of the CTV within columns, with right-handed columns composed exclusively of *R* enantiomers and left-handed columns composed exclusively of *S* enantiomers. The second process would be a partial deracemization of the CTV to form enantiomerically rich but not enantiomerically pure columns. These columns would contain an excess of one enantiomer, which would dictate the helical sense of the columns. As discussed previously, DSC and XRD experiments demonstrated that in the solid state the 50% (*S*)/50% (*R*) mixture forms helical columns whose enantiomeric purity can be enhanced by annealing at 60 °C. These results suggest that the columns formed in solution are helical, with equal contributions from left- and right-handed columns canceling each other. The enantiomeric purity of the columns in solution was further assessed in a majority-rules experiment to be discussed in a later subsection.

Even though the racemic and achiral dendronized CTV are CD silent, the UV absorption changes at 206 nm followed upon temperature changes give insight into the mechanism of self-assembly of these dendronized CTV as well as their chiral analogues. The absorption at the band maximum at 206 nm can be plotted versus temperature to determine whether self-assembly proceeds via an isodesmic or a cooperative mechanism following the method developed by the Schenning and Meijer laboratory.<sup>24</sup> In an isodesmic supramolecular polymerization process the association of each monomer to another monomer or to a growing chain occurs with the same equilibrium constant regardless of the length of the chain. By contrast, a cooperative self-assembly proceeds through two distinct steps: a nucleation or an activation step characterized by an equilibrium constant  $K_a$  and an elongation or growth step characterized by a higher equilibrium constant  $K_e$ .<sup>8i,j,25</sup> Typically nucleation consists of formation of the first turn or nucleus of the helix. Subsequent growth is facilitated once the nucleus is formed. The Meijer laboratory determined that isodesmic and cooperative self-assembly mechanisms can be distinguished by the curve profile of a temperature-dependent CD/UV experiment at a fixed wavelength.<sup>24</sup> The CD ellipticity or UV absorbance versus temperature is rescaled between 0 and 1 to reflect the degree of aggregation ( $\Phi$ ) of the self-assembling dendronized CTV. The curve profile obtained is characteristic of the mechanism of helical supramolecular polymerization. A sigmoidal curve corresponds to an isodesmic mechanism, whereas the presence of a sharp transition at  $\Phi \approx 0$  is distinctive of a cooperative mechanism. The transition occurs when growth of the supramolecular columns starts upon cooling. The corresponding temperature is referred to as the elongation temperature  $T_e$ . The curve of the degree of aggregation versus temperature can be modeled by eq 1 at temperatures below  $T_e$ .

$$\Phi = \Phi_{\text{SAT}} \left[ 1 - \exp\left(-\frac{h_e}{RT_e^2}(T - T_e)\right) \right] \quad (1)$$

where  $\Phi$  is the degree of aggregation,  $\Phi_{\text{SAT}}$  is the saturation level of the data,  $T$  is the temperature,  $T_e$  is the elongation

temperature,  $h_e$  is the molar enthalpy for supramolecular polymerization, and  $R$  is the gas constant.<sup>8i</sup>

The method described above was used to determine the mechanism of self-assembly of chiral and racemic (3,4)-dm8\*G1-CTV and the thermodynamics of their helical supramolecular polymerization. The absorbance of  $4.0 \times 10^{-5}$  M solutions of the CTV dendrimers in *n*-butanol at the maximum of the main absorption band (206 nm) was recorded upon cooling from 40 to  $-10$  °C at a slow rate of 0.5 °C/min, and the data at 206 nm were then converted to the degree of aggregation  $\Phi$  (Figure 11c). In all cases (*S* enantiomer, *R* enantiomer, racemic by mixing, and racemic by synthesis CTV) a sharp transition was observed between the molecularly dissolved state ( $\Phi = 0$ ) and the start of the self-assembly process ( $\Phi > 0$ ) with a sudden increase of the degree of aggregation. This sharp transition indicates a cooperative nucleation–elongation mechanism. Fitting of the experimental data with the elongation model from eq 1 generated the values of  $T_e$  and  $h_e$  reported in the inset of Figure 11c.

Note that in contrast to the spectra in Figure 11a (which were recorded in dodecane solution) the measurements illustrated in Figure 11c were performed in *n*-butanol solution. Experiments in dodecane gave similar cooling curves, but the elongation temperatures were low (down to 2 °C for the racemic by synthesis CTV), which made fitting calculations inaccurate (especially calculation of  $h_e$ ) because the temperature of the CD instrument could only be cooled down to  $-10$  °C and self-assembly was not complete at this temperature. CD and UV spectra of the self-assembled (3,4)dm8\*G1-CTV derived from enantiomerically pure or racemic samples are virtually identical in dodecane and *n*-butanol solutions (Figure SF6, Supporting Information), which indicates that the same supramolecular objects are formed in both solvents. Higher elongation temperatures in *n*-butanol made calculations more accurate, and therefore, this solvent was selected for this experiment.

Within experimental error the fitting results for the pure *S* enantiomer and for the pure *R* enantiomer are identical. Helical supramolecular polymerization of the enantiomerically pure CTV is an enthalpically driven process with  $h_e = -29 \pm 1$  kcal/mol that starts at the elongation temperature  $T_e = 29 \pm 1$  °C in *n*-butanol solution at a concentration of  $4.0 \times 10^{-5}$  M. Identical results are expected for the *S* and *R* enantiomers since the only difference between their self-assembled structures is the helix handedness. For the pure enantiomers the calculations can also be made from CD data and give similar results. However, in the present case the results obtained from UV data were selected for comparison with the racemic systems, which do not exhibit any CD signal.

When the *S* and *R* enantiomers are mixed in equimolar proportions to form the 50% (*S*)/50% (*R*) mixture or racemic by mixing, the enthalpy for supramolecular polymerization remains identical to that of pure enantiomers within experimental error. However, the elongation temperature of the racemic by mixing at a total dendrimer concentration of  $4.0 \times 10^{-5}$  M is lower than that of the enantiomerically pure self-assemblies: fitting calculations give  $T_e = 23$  °C for the racemic by mixing vs 28–29 °C for the pure enantiomers at the same concentration (Figure SF4, Supporting Information). These fitting results may be rationalized in light of the characterization of the 50% (*S*)/50% (*R*) mixture in the solid state. Annealing experiments revealed that the thermodynamic product in bulk consists of enantiomerically pure columns that are identical to

columns formed from pure enantiomers since they have matching DSC traces and XRD results. The constant enthalpy  $h_e$  observed for the 50% (*S*)/50% (*R*) mixture compared to pure enantiomers as well as the weakness of the majority-rules effect (discussed later) suggest that this deracemization process occurs in solution as well as in the solid state, although it is not perfect in solution. In this context deracemization occurs upon self-assembly, which means that the elongation is mostly homochiral (*S* enantiomers self-assemble with *S* enantiomers to form left-handed helical columns, and *R* enantiomers self-assemble with *R* enantiomers to form right-handed columns). Even if self-sorting is not perfect in solution, the enthalpy results and majority-rules experiment suggest that it is reasonable to assume that homochiral elongation is the predominant elongation mode. The self-sorting process implies that the effective concentration of each enantiomer available to build each type of column (left-handed or right-handed) in solution is only one-half of the total concentration of dendrimers. Therefore, in order to directly compare the elongation temperature of the 50% (*S*)/50% (*R*) mixture with the pure enantiomers, we need to consider a solution of the racemic mixture with a total concentration of  $8.0 \times 10^{-5}$  M, which corresponds to an effective concentration of  $4.0 \times 10^{-5}$  M for each enantiomer (identical to the concentration of the solutions of pure enantiomers used to calculate the elongation parameters). At this concentration we calculate an elongation temperature of 27 °C (Figure 11c) vs 28 °C for the pure *R* enantiomer and 29 °C for the pure *S* enantiomer. This result is consistent with the hypothesis that the enantiomers deracemize in solution, but self-sorting is not perfect and leads to a slight decrease of  $T_e$ .

Calculations for the self-assembly of the mixture of stereoisomers racemic by synthesis-(3,4)dm8\*G1-CTV give  $h_e = -13$  kcal/mol and  $T_e = 18$  °C. For this system both the enthalpy and the elongation temperature are lower than those of the pure enantiomers and 50% (*S*)/50% (*R*) mixture. These characteristics in solution are in good agreement with the conclusions of the solid state experiments. XRD and DSC of the racemic by synthesis sample showed significant loss of order in the 3D periodic array of supramolecular columns, which melt at a much lower temperature. These observations are in accordance with the lower enthalpy and elongation temperature obtained for the racemic by synthesis in solution. The loss of order in the self-assembled structure is demonstrated by the fact that columns of the racemic by synthesis dendronized CTV are less thermally stable than the columns formed by the pure enantiomers or the racemic by mixture and that their formation is not as enthalpically favorable. Moreover, the clear differences observed between  $h_e$  and  $T_e$  of the racemic by synthesis CTV and the 50% (*S*)/50% (*R*) mixture confirm that the enantiomerically pure compounds play an important role in facilitating and stabilizing formation of helical supramolecular columns.

The temperature-dependent CD/UV experiments were performed at a slow cooling rate of 0.5 °C/min to ensure that the system always remained at thermodynamic equilibrium. However, a hysteresis was systematically observed between cooling and heating cycles. Attempts to slow down the heating/cooling rate did not eliminate the hysteresis, even at 0.08 °C/min. However, it was observed that the heating curves are affected by the heating rate, while the cooling curves remained essentially unaffected. This result suggests that kinetic effects affect the dissociation of the self-assembled columns upon

heating, whereas the cooling curves reflect the thermodynamic self-assembly process. This hypothesis was confirmed by two "temperature-hold" experiments. In a first experiment, a  $8.0 \times 10^{-5}$  M solution of (*S*)-(3,4)dm8\*G1-CTV was cooled down from 50 to 25 °C (which is the center temperature of the hysteresis cycle), whereupon the temperature was held, and CD changes with time were monitored at 240 nm. The ellipticity did not change over time and remained close to zero ellipticity (0 mdeg), which confirms that the thermodynamic state of the system at this temperature is the molecularly dissolved state and not the self-assembled state. In a second experiment, the solution was heated at a rate of 0.5 °C/min from the self-assembled state at 0–25 °C, whereupon the temperature was held. Slow changes in the CD signal were observed over time, and the ellipticity slowly decreased to reach nearly 0 mdeg after 90 h (Figure SF7, Supporting Information). The decrease in ellipticity reflects a slow dissociation of the self-assembled columns over time, which demonstrates that the self-assembled state is thermodynamically unstable at 25 °C but the kinetics of dissociation are very slow. Overall, the temperature-hold experiments indicate that cooling scans reflect the thermodynamic behavior of the system, while the data obtained from heating scans are affected by kinetic effects and are therefore not suitable for thermodynamic calculations. Consequently, data from cooling scans were exclusively used for fitting with the elongation equation and calculation of the enthalpy for supramolecular polymerization.

It is also important to note that eq 1 is based on a helical self-assembly model that involves only supramolecular polymerization of identical monomers. This model is suitable for the enantiomerically pure dendronized CTV. However, self-assembly of the racemic systems (racemic by mixing and racemic by synthesis) does not exactly correspond to the type of system for which the model was developed. For example, supramolecular polymerization of the racemic by mixing involves two distinct monomers (the *S* and *R* enantiomers), which can potentially form different types of assemblies, right-handed and left-handed helical columns or columns with no well-defined helicity. However, the two types of monomers differ only in the stereochemistry of their peripheral alkyl chains, and their self-assembly involves many supramolecular interactions over the whole surface of the dendronized CTV. Therefore, we can reasonably assume that the differences between the equilibrium constants of monomer additions to growing chains are small compared to the order of magnitude of the equilibrium constants. In other words, we assume that the equilibrium constants are approximately the same for each monomer addition to each type of column, and we use the same elongation model in all cases. This assumption is supported by the good fit between the experimental curve profile and the model.

In order to gain more insight into the thermodynamics of the helical supramolecular polymerization, temperature-dependent CD/UV experiments were performed at different concentrations in *n*-butanol. Determining the elongation temperature  $T_e$  at different concentrations of dendronized CTV allowed calculation of both the enthalpy  $h_e$  and the molar entropy  $s_e$  that characterize the elongation step in the cooperative self-assembly process. These thermodynamic parameters were obtained from a van't Hoff plot.<sup>81</sup> For example, the data obtained for the pure *S* enantiomer of (3,4)dm8\*G1-CTV gave  $h_e = -44$  kcal·mol<sup>-1</sup> and  $s_e = -126$  cal·mol<sup>-1</sup>·K<sup>-1</sup> (Figure SF8, Supporting Information). The value of  $h_e$  calculated from the

van't Hoff plot is higher than the value obtained by fitting of the cooling data at  $4.0 \times 10^{-5}$  M with the elongation equation ( $h_e = -29 \text{ kcal.mol}^{-1}$ ). This difference and dependence on the wavelength used for calculation discussed in the Supporting Information indicate that the enthalpy and entropy cannot be determined with great precision using these methods. However, the sign and order of magnitude of the enthalpy obtained using both methods are the same and correspond to the expected thermodynamic behavior. The respective signs of the enthalpy and entropy indicate that the self-assembly of dendronized CTV molecules is an enthalpically driven process. Supramolecular polymerization is enthalpically favored and entropically disfavored. The enthalpic contribution predominates below the elongation temperature  $T_e$ , while the entropic contribution promotes dissociation of the columns above  $T_e$ . van't Hoff plots were also obtained for both racemic systems (the racemic by mixing and the racemic by synthesis (3,4)dm8\*G1-CTV). The results were similar to those obtained for the *S* enantiomer, which suggests that the differences in enthalpy and entropy between these systems are too small to be accurately determined from van't Hoff plots. However, the clear trend observed for the elongation temperature, which decreases from the pure enantiomers to the racemic by mixing to the racemic by synthesis, demonstrates the differences in thermal stability between these systems and proves that chirality facilitates the self-assembly of dendronized CTV.

**Majority-Rules Experiment.** A majority-rules experiment<sup>26</sup> was performed (Figure 11d and 11e) in order to elucidate the effect of mismatched chirality on the self-assembly of CTV dendrimers. This experiment consists of comparing the Cotton effects of solutions that contain various proportions of *S* and *R* units in a helical polymer or supramolecular polymer. In the absence of a majority-rules effect the ratio of left-handed vs right-handed helices should be identical to the ratio of *S* vs *R* enantiomers and a linear response is expected. The ellipticity at a given wavelength is proportional to the enantiomer excess. However, if the system exhibits a majority-rules effect, a nonlinear response is observed and the ellipticity should exceed the expected linear behavior. This nonlinear effect occurs if the major enantiomer can dictate its preferred helical sense to the minor enantiomer and the “wrong” enantiomer can be inserted into a helical supramolecular column without disturbing its helicity. In order to investigate the majority-rules effect in the self-assembly of CTV dendrimers, CD spectra of solutions of (*S*)- and (*R*)-(3,4)dm8\*G1-CTV (total concentration of  $4.0 \times 10^{-5}$  M in dodecane) mixed in various proportions were measured at 0 °C after slow cooling (0.5 °C/min) from the molecularly dissolved state at 50 °C. The CD spectra and net helicity (obtained from the ellipticity at 289 nm) vs enantiomeric excess are depicted in Figure 11d and 11e. Although the effect is not very intense under these conditions in this solvent, we observe a deviation from linearity and the net helicity slightly outpaces the enantiomeric excess. As discussed in previous sections of this study, mixtures of enantiomers of dendronized CTV tend to deracemize to form enantiomerically pure columns. If the deracemization process was perfect then no majority-rules effect should be observed because left-handed columns should contain exclusively *S* enantiomers and right-handed columns exclusively *R* enantiomers. Therefore, the ratio of left- vs right-handed columns, and hence the net helicity, should be proportional to the enantiomeric excess. The weak majority-rules effect observed here supports previously

discussed results on deracemization but indicates that this process is not complete in solution.

**Microspot CD Analysis of Thin Films.** Although almost no net helicity was observed in racemized samples obtained by mixing or by synthesis in solution by CD measurements, it is of interest to understand whether the self-assemblies are racemized within the column or in between columns as already suggested by XRD results, that is, we wish to determine whether individual supramolecular columns are helical and single handed but Cotton effects are macroscopically canceled due to opposite contributions or individual columns are racemized along the column and have poorly defined helicities. Since solution CD experiments only provide averaged information within a relatively large solution volume, signals from individual columns are not accessible. In order to obtain chiral information from monodomains that might show preference of helical sense, a microspot CD setup equipped with ultrasmall beam size, less than a few hundred micrometers, was used to examine solid state thin films made of racemic and achiral samples (Figure 12). Thin films of fully racemized or racemic by synthesis (3,4)dm8\*G1-CTV and achiral (3,4)8G1-CTV with linear 8-carbon side chains were prepared on a quartz plate by spin coating from 2% w/v chloroform solutions followed by melting at 85 °C and slow cooling to RT for development of the  $\Phi_h^k$  structure. Note that the birefringence of these films observed by polarized microscopy was confirmed

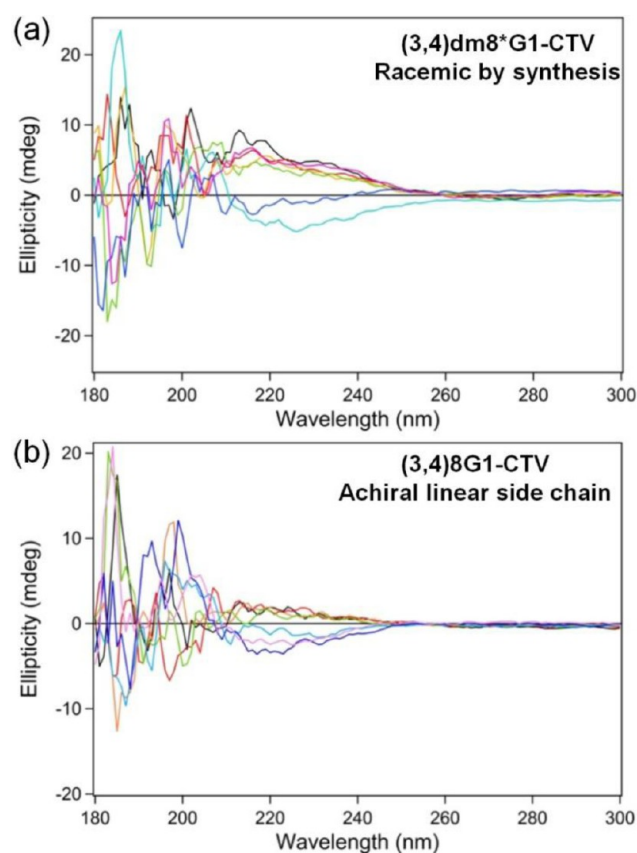


**Figure 12.** Thin film micro-CD spectra of (a) racemic by synthesis (3,4)dm8\*G1-CTV and (b) (3,4)8G1-CTV with achiral 8-carbon linear side chains collected in the  $\Phi_h^k$  phase at room temperature. Films were spin coated on a quartz plate followed by melting at 85 °C and subsequent cooling to room temperature. Each spectrum was obtained from different spots on the film.

to be negligibly small. Each curve in Figure 12 represents a single measurement at one microspot on the film. The signal from wavelengths below 200 nm is affected by the quartz substrate and shows irregular patterns that should be ignored. Signals from the dendronized CTVs are located between 200 and 250 nm. Figure 12a shows the results from the film made of racemic by synthesis sample. Here the 12 side chains with either *R* or *S* chiral center are randomly arranged on each molecule and lead to no preference of rotation sense during column assembly and therefore show zero net helicity in solution CD measurements.

Nevertheless, opposite signs of ellipticity were observed at different microspots in the thin film (Figure 12a). This confirms formation of monodomains consisting of right- and left-handed columns and suggests that a spontaneous deracemization process involves diffusion between columns and that the column handedness is most probably decided at the nucleation step. Although the columns seem to possess selected handedness, the phase separation of columns with opposite handedness is weak and therefore results in very small domain size. The mixing of right- and left-handed columns prevents formation of 3D ordered crystals and generates both inter- and intracolumn packing defects as evidenced by very weak CD signals and low melting temperatures found in the DSC of the as-prepared samples.

Similar microspot CD experiments were also conducted on a thin film of achiral (3,4)8G1-CTV with linear achiral 8-carbon side chains (Figure 12b). Surprisingly, although the intensity was even weaker than its chiral analogue, positive or negative net ellipticity was still observed from spot to spot. This suggests that the spontaneous deracemizing of supramolecular columns occurs even in achiral CTVs, and the overall film is racemic because of the mixing of right- and left-handed columns. The even weaker CD intensities indicate the random distribution of right- and left-handed columns throughout the film, and the monodomain size is much smaller than the beam size. The random distribution of columns results in less perfect crystals at room temperature as evidenced by the observation of fewer and weaker quadrant reflections in XRD patterns.

From the above discussion, we concluded that all CTV samples self-assemble into chiral nonracemic supramolecular columns since even achiral compound forms domains with single chirality. Microphase separation of columns with different handedness generates separated crystalline domains. Therefore, racemic samples are racemized between domains, not within each column. However, the phase separation strength is not strong in the bulk state and results in small domain sizes that give weak CD intensities. The handedness is determined at an early stage of column formation, the nucleation step. Once the handedness is decided by the first few molecules, the next molecule will follow the same rotation sense during the elongation step even if the rotation sense is not preferred by the molecule, since making an opposite rotation in an existing column would cost more energy and is not favored. Therefore, the supramolecular columns are not enantiomerically pure but are of single handedness. The molecules forced to stack in columns with nonfavored rotation will not be able to pack perfectly with molecules in neighboring columns, creating defects in the crystal by destroying the correlation between columns. The melting temperature is determined by the defect density in the crystal.

## CONCLUSIONS

Synthesis and self-organization of a library based on five self-assembling dendronized cyclotriveratrylenes (CTV) with *R* and *S* side chain chirality containing various combinations of *R* with *S* including racemic by mixing and racemic by synthesis as well as achiral analogues with *n*-octyl and *n*-dodecyl side chains was reported. The structures of all assemblies generated from these dendronized CTV that are shape persistent in solution and in bulk were determined by a combination of complementary techniques including CD-UV in solution and thin film, microspot CD in thin film, DSC, fiber XRD, and computer simulation of molecular models of the oriented fiber XRD to reveal the mechanisms of self-assembly, racemization, and deracemization during their helical supramolecular polymerization in solvophobic solvents and in their 3D  $\Phi_h^k$  and 2D  $\Phi_h$  phases. Supramolecular columns self-assemble in solution through a cooperative nucleation–elongation mechanism with enthalpies ranging from 29 kcal/mol for enantiopure and racemic by mixture dendronized CTV to 18 kcal/mol for racemic by synthesis CTV. These values are lower than those of previously investigated dendritic dipeptides that range from 35 to 19 kcal/mol and did not undergo deracemization in bulk.<sup>1c,12</sup> The enantiopure dendronized CTVs self-assemble into single-handed columns, while racemic mixtures are generated from equal ratios of left- and right-handed supramolecular columns that can be considered a homochiral supramolecular polymerization.<sup>8d,e</sup> No intracolumnar racemization was detected in any of these chiral, chiral racemic, or achiral compositions; in other words, the self-assembled columns are single-handed helical in all cases. Even columns generated from achiral dendronized CTV and racemic by synthesis CTV exhibit single handedness in their  $\Phi_h^k$  monodomains. Since  $\Phi_h^k$  monodomains can be generated only from columns of single handedness, the order of the  $\Phi_h^k$  crystals is determined by the enantiomeric purity of their single-handed columns. Therefore, deracemization of single-handed columns containing different enantiomeric compositions, including racemic, could be monitored by annealing in the crystal state at 60 °C. Solid state NMR experiments demonstrated that column deracemization occurs via the exit and reentry of the disc-like transient conformer of the hat-shaped dendronized CTV that is available during the crown to crown inversion. Overall, these results reveal that supramolecular chirality, at least in columnar architectures, can be generated from racemic and even achiral building blocks. They also demonstrate again<sup>1c,12</sup> that when chirality is present homochirality is essential in formation of highly ordered, stable, and 3D  $\Phi_h^k$  crystalline assemblies. However, when deracemization is accessible, it can transform mixtures of left-handed and right-handed columns containing different enantiomeric purities including racemic and achiral into highly ordered single domains of enantiopure single-handed columns. Homochiral supramolecular polymerization of racemic mixtures was previously reported only in solution for rigid S-shape and rigid macrocycles as well as for disc-like compounds with an exceedingly high number of stereogenic centers.<sup>8d–f</sup> However, spontaneous deracemization or chiral self-sorting of supramolecular columns obtained from various enantiomeric ratios including racemic and from achiral building blocks, to our best knowledge, has been demonstrated for the first time in their crystal state in this publication. Elucidating the molecular principles to realize chiral self-sorting at the supramolecular level in the crystal state will have numerous technological

applications in complex systems where perfection of crystal structure mediates functions. Finally, a parallel can be drawn with the homochirality of the molecules of life. Our results suggest that systems composed of chiral or even homochiral building blocks lead to more stable, more ordered, and thus more perfectly functional structures. This gives again insight into the reasons why nature selected and retained homochirality during its evolution.

## ■ ASSOCIATED CONTENT

### ● Supporting Information

Experimental procedures and methods with complete spectral and structural analysis. This material is available free of charge via the Internet at <http://pubs.acs.org>.

## ■ AUTHOR INFORMATION

### Corresponding Author

percec@sas.upenn.edu

### Notes

The authors declare no competing financial interest.

## ■ ACKNOWLEDGMENTS

Financial support by the National Science Foundation (DMR-1066116 and DMR-1120901), the Humboldt Foundation, and the P. Roy Vagelos Chair at Penn (all to V.P.) is gratefully acknowledged. G.U. and X.Z. acknowledge support from the joint NSF-EPSRC PIRE project "RENEW" (EPSRC grant EP-K034308).

## ■ REFERENCES

- (1) (a) Frank, P.; Bonner, W. A.; Zare, R. N. In *Chemistry for the 21st Century*; Keinan, E., Schechter, I., Ed.; Wiley-VCH: Weinheim, 2001; pp 175–202. (b) Gal, J.; Cintas, P. *Top. Curr. Chem.* **2013**, *333*, 1–40. (c) Rosen, B. M.; Roche, C.; Percec, V. *Top. Curr. Chem.* **2013**, *333*, 213–254. (d) Breslow, R. *Isr. J. Chem.* **2011**, *51*, 990–996. (e) Weissbuch, I.; Lahav, M. *Chem. Rev.* **2011**, *111*, 3236–3267. (f) Hein, J. E.; Gherase, D.; Blackmond, D. G. *Top. Curr. Chem.* **2013**, *333*, 83–108.
- (2) (a) Nicolaou, K. C.; Sorensen, E. J. *Classics in Total Synthesis*; Wiley-VCH: Weinheim, 1996. (b) Nicolaou, K. C.; Snyder, S. A. *Classics in Total Synthesis II*; Wiley-VCH: Weinheim, 2003. (c) Nicolaou, K. C.; Montagnon, T. *Molecules That Changed the World*; Wiley-VCH: Weinheim, 2008. (d) Stinson, S. C. *Chem. Eng. News* **2001**, *79* (40), 79–97.
- (3) (a) Pasteur, L. *Ann. Chim. Phys.* **1848**, *24*, 442–459. (b) Jacques, J.; Collet, A.; Wilen, S. H. *Enantiomers, Racemates and Resolutions*; Krieger Pub. Co.: Malabar, FL, 1991.
- (4) (a) Nagayama, H.; Varshney, S. K.; Goto, M.; Araoka, F.; Ishikawa, K.; Prasad, V.; Takezoe, H. *Angew. Chem., Int. Ed.* **2010**, *122*, 455–458. (b) Link, D. R.; Natale, G.; Shao, R.; MacLennan, J. E.; Clark, N. A.; Körblöva, E.; Walba, D. M. *Science* **1997**, *278*, 1924–1927.
- (5) (a) Okamoto, Y.; Yashima, E. *Angew. Chem., Int. Ed.* **1998**, *37*, 1020–1043. (b) Nakano, T.; Okamoto, Y. *Chem. Rev.* **2001**, *101*, 4013–4038. (c) Okamoto, Y. *Adv. Polym. Sci.* **2013**, *261*, 391–414.
- (6) (a) Knowles, W. S. *Angew. Chem., Int. Ed.* **2002**, *41*, 1998–2007. (b) Noyori, R. *Angew. Chem., Int. Ed.* **2002**, *41*, 2008–2022. (c) Sharpless, K. B. *Angew. Chem., Int. Ed.* **2002**, *41*, 2024–2032.
- (7) (a) Brienne, M.-J.; Gabard, J.; Lehn, J.-M.; Stibor, I. *J. Chem. Soc., Chem. Commun.* **1989**, 1868–1870. (b) Fouquey, C.; Lehn, J.-M.; Levelut, A.-M. *Adv. Mater.* **1990**, *2*, 254–257. (c) Gulik-Krzywicki, T.; Fouquey, C.; Lehn, J. *Proc. Natl. Acad. Sci. U.S.A.* **1993**, *90*, 163–167. (d) Lehn, J.-M. *Angew. Chem., Int. Ed.* **1988**, *27*, 89–112. (e) Percec, V.; Heck, J.; Lee, M.; Ungar, G.; Alvarez-Castillo, A. *J. Mater. Chem.* **1992**, *2*, 1033–1039. (f) Percec, V.; Johansson, G.; Heck, J.; Ungar,

G.; Batty, S. V. *J. Chem. Soc., Perkin Trans. 1* **1993**, 1411–1420. (g) Percec, V.; Heck, J.; Tomazos, D.; Falkenberg, F.; Blackwell, H.; Ungar, G. *J. Chem. Soc., Perkin Trans. 1* **1993**, 2799–2811. (h) Johansson, G.; Percec, V.; Ungar, G.; Abramic, D. *J. Chem. Soc., Perkin Trans. 1* **1994**, 447–459. (i) Kwon, Y. K.; Chvalun, S.; Schneider, A.-I.; Blackwell, J.; Percec, V.; Heck, J. A. *Macromolecules* **1994**, *27*, 6129–6132. (j) Percec, V.; Heck, J.; Johansson, G.; Tomazos, D.; Kawasumi, M.; Ungar, G. *J. Macromol. Sci., Pure Appl. Chem.* **1994**, *A31*, 1031–1070. (k) Engelkamp, H.; Middelbeek, S.; Nolte, J. M. R. *Science* **1999**, *284*, 785–788. (l) Malthête, J.; Jacques, J.; Tinh, N. H.; Destrade, C. *Nature* **1982**, *298*, 46–48. (m) Percec, V.; Ahn, C.-H.; Bera, T. K.; Ungar, G.; Yeardley, D. J. P. *Chem.—Eur. J.* **1999**, *5*, 1070–1083.

(8) (a) Addadi, L.; Weiner, S. *Nature* **2001**, *411*, 753–755. (b) Snir, Y.; Kamien, R. D. *Science* **2005**, *307*, 1067. (c) Pokroy, B.; Kang, S. H.; Mahadevan, L.; Aizenberg, J. *Science* **2009**, *323*, 237–240. (d) Ishida, Y.; Aida, T. *J. Am. Chem. Soc.* **2002**, *124*, 14017–14019. (e) Sato, K.; Itoh, Y.; Aida, T. *Chem. Sci.* **2014**, *5*, 136–140. (f) Wolffs, M.; van Velthoven, J. L. J.; Lou, X.; Bovee, R. A. A.; Pouderoijen, M.; van Dongen, J. L. J.; Schenning, A. P. H. J.; Meijer, E. W. *Chem.—Eur. J.* **2012**, *18*, 15057–15064. (g) Jin, W.; Fukushima, T.; Niki, M.; Kosaka, A.; Ishii, N.; Aida, T. *Proc. Natl. Acad. Sci. U.S.A.* **2005**, *102*, 10801–10806. (h) van Gestel, J.; Palmans, A. R. A.; Titulaer, B.; Vekemans, J. A. J. M.; Meijer, E. W. *J. Am. Chem. Soc.* **2005**, *127*, 5490–5494. (i) Jonkheijm, P.; van der Schoot, P.; Schenning, A. P. H. J.; Meijer, E. W. *Science* **2006**, *313*, 80–83. (j) Percec, V.; Ungar, G.; Peterca, M. *Science* **2006**, *313*, 55–56. (k) Korevaar, P. A.; George, S. J.; Markvoort, A. J.; Smulders, M. M. J.; Hilbers, P. A. J.; Schenning, A. P. H. J.; De Greef, T. F. A.; Meijer, E. W. *Nature* **2012**, *481*, 492–496. (l) Pérez-García, L.; Amabilino, D. B. *Chem. Soc. Rev.* **2007**, *36*, 941–967. (m) Fasel, R.; Parschau, M.; Ernst, K.-H. *Nature* **2006**, *439*, 449–452. (n) Safont-Sempere, M. M.; Fernández, G.; Würthner, F. *Chem. Rev.* **2011**, *111*, 5784–5814. (o) Fletcher, S. P.; Jagt, R. B. C.; Feringa, B. L. *Chem. Commun.* **2007**, 2578–2580. (p) Sisco, S. W.; Moore, J. S. *Chem. Sci.* **2014**, *5*, 81–85.

(9) (a) Lehn, J.-M. *Proc. Natl. Acad. Sci. U.S.A.* **2002**, *99*, 4763–4768. (b) Rosen, B. M.; Wilson, C. J.; Wilson, D. A.; Peterca, M.; Imam, M. R.; Percec, V. *Chem. Rev.* **2009**, *109*, 6275–6540. (c) Rudick, J. G.; Percec, V. *Acc. Chem. Res.* **2008**, *41*, 1641–1652. (d) Rowan, A. E.; Nolte, R. J. M. *Angew. Chem., Int. Ed.* **1998**, *37*, 63–68. (e) Elemans, J. A. A. W.; Rowan, A. E.; Nolte, R. J. M. *J. Mater. Chem.* **2003**, *13*, 2661–2670. (f) Korevaar, P. A.; de Greef, T. F. A.; Meijer, E. W. *Chem. Mater.* **2013**, *26*, 576–586.

(10) (a) Percec, V.; Glodde, M.; Bera, T. K.; Miura, Y.; Shiyonovskaya, I.; Singer, K. D.; Balagurusamy, V. S. K.; Heiney, P. A.; Schnell, I.; Rapp, A.; Spiess, H.-W.; Hudson, S. D.; Duan, H. *Nature* **2002**, *417*, 384–387. (b) Percec, V.; Peterca, M.; Tadjiev, T.; Zeng, X.; Ungar, G.; Leowanawat, P.; Aqad, E.; Imam, M. R.; Rosen, B. M.; Akbey, U.; Graf, R.; Sekharan, S.; Sebastiani, D.; Spiess, H. W.; Heiney, P. A.; Hudson, S. D. *J. Am. Chem. Soc.* **2011**, *133*, 12197–12219. (c) Percec, V.; Hudson, S. D.; Peterca, M.; Leowanawat, P.; Aqad, E.; Graf, R.; Spiess, H. W.; Zeng, X.; Ungar, G.; Heiney, P. A. *J. Am. Chem. Soc.* **2011**, *133*, 18479–18494. (d) Percec, V.; Sun, H.-J.; Leowanawat, P.; Peterca, M.; Graf, R.; Spiess, H. W.; Zeng, X.; Ungar, G.; Heiney, P. A. *J. Am. Chem. Soc.* **2013**, *135*, 4129–4148. (e) Würthner, F.; Stolte, M. *Chem. Commun.* **2011**, *47*, 5109–5115.

(11) Percec, V.; Dulcey, A. E.; Balagurusamy, V. S. K.; Miura, Y.; Smidrkal, J.; Peterca, M.; Nummelin, S.; Edlund, U.; Hudson, S. D.; Heiney, P. A.; Duan, H.; Magonov, S. N.; Vinogradov, S. A. *Nature* **2004**, *430*, 764–768.

(12) (a) Rosen, B. M.; Peterca, M.; Morimitsu, K.; Dulcey, A. E.; Leowanawat, P.; Resmerita, A.-M.; Imam, M. R.; Percec, V. *J. Am. Chem. Soc.* **2011**, *133*, 5135–5151. (b) Percec, V.; Leowanawat, P. *Isr. J. Chem.* **2011**, *51*, 1107–1117.

(13) (a) Percec, V.; Imam, M. R.; Peterca, M.; Wilson, D. A.; Heiney, P. A. *J. Am. Chem. Soc.* **2009**, *131*, 1294–1304. (b) Malthête, J.; Collet, A. *J. Am. Chem. Soc.* **1987**, *109*, 7544–7545.

(14) Peterca, M.; Percec, V.; Imam, M. R.; Leowanawat, P.; Morimitsu, K.; Heiney, P. A. *J. Am. Chem. Soc.* **2008**, *130*, 14840–14852.

(15) Shcherbina, M. A.; Zeng, X.-b.; Tadjiev, T.; Ungar, G.; Eichhorn, S. H.; Phillips, K. E. S.; Katz, T. *J. Angew. Chem., Int. Ed.* **2009**, *48*, 7837–7840.

(16) (a) Zerbi, G.; Magni, R.; Gussoni, M.; Moritz, K. H.; Bigotto, A.; Dirlikov, S. *J. Chem. Phys.* **1981**, *75*, 3175–3194. (b) Maroncelli, M.; Qi, S. P.; Strauss, H. L.; Snyder, R. G. *J. Am. Chem. Soc.* **1982**, *104*, 6237–6247.

(17) (a) Watson, J. D.; Crick, F. H. C. *Nature* **1953**, *171*, 964–967. (b) Cochran, W.; Crick, F. H.; Vand, V. *Acta Crystallogr.* **1952**, *5*, 581–586. (c) Lucas, A. A.; Lambin, P.; Mairesse, R.; Mathot, M. J. *Chem. Educ.* **1999**, *76*, 378–383.

(18) Schmidt-Rohr, K.; Spiess, H. W. *Multidimensional Solid-State NMR and Polymers*; Academic Press: New York, 1994.

(19) Demus, D.; Goodby, J. W.; Gray, G. W.; Spiess, H. W.; Vill, V. *Handbook of Liquid Crystals*; Wiley-VCH: Weinheim, 1998; Vol. 1 (Fundamentals).

(20) Elmahdy, M. M.; Floudas, G.; Mondeshki, M.; Spiess, H. W.; Dou, X.; Müllen, K. *Phys. Rev. Lett.* **2008**, *100*, 107801.

(21) Dong, R. Y.; Goldfarb, D.; Moseley, M. E.; Luz, Z.; Zimmermann, H. *J. Phys. Chem.* **1984**, *88*, 3148–3152.

(22) Floudas, G.; Spiess, H. W. *Macromol. Rapid Commun.* **2009**, *30*, 278–298.

(23) (a) Harada, N.; Nakanishi, K. *Acc. Chem. Res.* **1972**, *5*, 257–263. (b) Takei, F.; Hayashi, H.; Onitsuka, K.; Kobayashi, N.; Takahashi, S. *Angew. Chem., Int. Ed.* **2001**, *40*, 4092–4094. (c) Berova, N.; Bari, L. D.; Pescitelli, G. *Chem. Soc. Rev.* **2007**, *36*, 914–931. (d) Percec, V.; Peterca, M.; Rudick, J. G.; Aqad, E.; Imam, M. R.; Heiney, P. A. *Chem.—Eur. J.* **2007**, *13*, 9572–9581.

(24) Smulders, M. M. J.; Nieuwenhuizen, M. M. L.; de Greef, T. F. A.; van der Schoot, P.; Schenning, A. P. H. J.; Meijer, E. W. *Chem.—Eur. J.* **2010**, *16*, 362–367.

(25) De Greef, T. F. A.; Smulders, M. M. J.; Wolffs, M.; Schenning, A. P. H. J.; Sijbesma, R. P.; Meijer, E. W. *Chem. Rev.* **2009**, *109*, 5687–5754.

(26) Green, M. M.; Garetz, B. A.; Munoz, B.; Chang, H.; Hoke, S.; Cooks, R. G. *J. Am. Chem. Soc.* **1995**, *117*, 4181–4182.